

1 **RC1:**

2 China is one of the largest agricultural countries in the world. The NH₃ emissions from agricultural
3 activities in China, such as fertilizer and husbandry, farmland ecosystems, livestock waste, crop residue
4 burning and fuel wood combustion, significantly affect regional air quality and horizontal visibility by
5 contribution to secondary inorganic aerosols. In the manuscript, the air quality modeling system RAMS-
6 CMAQ (regional atmospheric modeling system-community multiscale air quality), coupled with the ISAM
7 (integrated source apportionment method) module is applied to capture the contribution of NH₃ emitted
8 from total agriculture (Tagr) in China. It explores that the annual average contribution of Tagr NH₃ to
9 PM_{2.5} mass burden in China was 14-18%. Specific to the PM_{2.5} components, Tagr NH₃ provided a major
10 contribution to ammonium formation (87.6%) but a tiny contribution to sulfate (2.2%). Though the Tagr
11 NH₃ only contributed 10.1% of nitrate under current emissions scenarios, the reduction of nitrate could
12 reach 98.8% upon removal of the Tagr NH₃ emissions. The results are meaningful, but the explanation for
13 these phenomenon was not enough. I recommend the manuscript to be accepted after some minor revisions,
14 and detail some issues below.

15 Major points:

16 *1. The most important gas in this manuscript was NH₃, but there are no NH₃ in Figure 2 in comparing*
17 *between the modeled and observed results.*

18 R: Thanks for this comment. However, NH₃ is not included in the routine measurement species in China at
19 present. Therefore, it is hard to collect available observation data of NH₃ mass concentration for model
20 evaluation directly. Most of the available information was derived from the published research paper. In
21 Han et al. (2017; Modeling dry deposition of reactive nitrogen in China with RAMS-CMAQ. Atmos.
22 Environ.), the simulated NH₃ by RAMS-CMAQ has been compared with the observations from many
23 studies in detail, including the multi-year observation results with Nationwide Nitrogen Deposition
24 Monitoring Network and the seasonal variation data from Pan et al. (2012; Wet and dry deposition of
25 atmospheric nitrogen at ten sites in Northern China. Atmos. Chem. Phys.). In this paper, we also compare
26 the simulation results with the observation data at several stations from Pan et al. (2018) and Zhang et al.
27 (2018) (Line 200-211). We kindly hope these content could reflect the reasonability of modeled NH₃.

28

29 *2. Why is the NH₃ contribution to nitrate small under "rich NH₃" conditions and large in "poor NH₃"*
30 *environments? What is the internal logical relationship?*

31 R: Thanks for this comment. In fact, the earlier discussion about "rich NH₃" and "poor NH₃" can be found
32 in Wang et al. (2011; Impact Assessment of Ammonia Emissions on Inorganic Aerosols in East China Using
33 Response Surface Modeling Technique). The results of RSM (Response Surface Modeling) in their study
34 shows that the change of NO₃⁻ mass concentration is very sensitive to the emission level of NH₄⁺ and
35 performs as nonlinear relationship. The reduction of NH₃ emissions can play a significant role in reducing
36 the mass concentration of NO₃⁻ under NH₃-poor condition. However, there will be excess NH₃ in the
37 atmosphere under NH₃-rich condition, and these excess NH₃ could neutralizes more nitric acid even in the
38 case of emission reduction. Thus, the effect of emission reduction is not significant under NH₃-rich
39 condition. In addition, the SO₂ will compete for NH₃ and prevent the generation of NH₄NO₃ under NH₃-
40 poor condition because the reaction between H₂SO₄ and NH₃ takes precedence over the one between HNO₃
41 and NH₃. Oppositely, SO₂ should be benefit for the formation of NO₃⁻ (especially in summer) under NH₃-
42 rich condition according to the calculation of Wang et al. (2011). This should be another reason why the
43 effect of NH₃ emission control is not obvious in the case of NH₃-rich condition.

44

45 *3. The study period is January, April, July, and October, but only the modeled and observed results in*
46 *January and July are compared in Figure A1, A2, A3 and A4.*

47 R: Thanks for this comment. We added the comparison of meteorological factors in April and October.
48 Please check if it is appropriate.

49

50 *4. The author thinks that the obvious deviation between the observed and modeled SO₂ in January may be*
51 *a systemic underestimation due to the lack of emission intensity in this month. Did the lack of emission*
52 *intensity only appear in SO₂? Why are SO₂ and NO₂ underestimated and PM_{2.5} overestimated?*

53 R: Thanks for this comment. The monthly mean observation data were used in the previous submitted
54 version. However, we would like to provide more details about the evaluation. Thus, these content is
55 modified. The hourly observation data from the China National Environmental Monitoring Centre were
56 collected and compared with simulation results. The scatter plots (Figure 2) were replaced and the
57 comparison of SO₂, NO₂ and PM_{2.5} in January, April, July, and October at six sites were presented, and the
58 statistical summary of the comparisons and related discussion were modified (Line 186-198). Please check
59 if it is appropriate.

60

61 *5. How much NH₃ is removed in Figure 7? And it's more intuitive to use a negative value for reduction.*

62 R: Thanks for this comment. Here the emission of NH₃ from all agricultural sources were removed. For
63 detail information, please see the percentage shown in Figure A6 which we added. In addition, the
64 horizontal distribution of the PKU-NH₃ emission inventory can be viewed in Kang et al. (2016) (Kang et
65 al., 2016: High-resolution ammonia emissions, High-resolution, ammonia 1980, 2012.). On the other hand,
66 the Figure 7 was also modified. Please check if it is appropriate.

67

68 *6. Why do the trend of the decrease in ammonium mass concentration accelerate while NH₃ emissions is
69 less than 20%?*

70 R: Thanks for this comment. Here the interval of simulation scenario conducted for emission reduction was
71 10%, so that the acceleration should appear between 20% and 30%. In fact, it can be found that the
72 accelerated decline mainly started when the emission reduction exceeds 50%. Therefore, we could deduce
73 that the accelerated decline should be emerged gradually with NH₃ emission reduction. This feature
74 indicates that the formation of NH₄⁺ should be nonlinear with NH₃ emission intensity as well. The reason
75 may also be related to the complex neutralization reaction among sulfate, nitrate and ammonium. The
76 consumption of NH₃ should become more sufficient when the mass concentration of NH₃ is lower. Thus,
77 the variation of ammonium is more sensitive under low NH₃ mass burden.

78

79 *7. What is the horizontal distributions of the contribution percentage of NH₃ emissions to ammonium,
80 nitrate and sulfate mass concentration, respectively? Which aerosol determines the horizontal distributions
81 of SNA mass concentration? Why is the horizontal distributions of NH₃ emissions different with the
82 horizontal distributions of the contribution percentage of NH₃ emissions to SNA mass concentration?*

83 R: Thanks for this comment. The horizontal distributions of NH₃ emission contribution to sulfate, nitrate
84 and ammonium is shown in Figure R1, and the major contribution was provided by ammonium (Table 4
85 also presented related information). In addition, Figure 6 shows the horizontal distributions of contribution
86 percentage which may not follow the distribution pattern of mass concentration. For example, it can be seen
87 that the agricultural NH₃ emission generally provided more than 70% contribution to ammonium formation
88 over China as shown in Figure R1, and the horizontal distribution pattern of contribution ratio was
89 obviously different from that of the mass burden.

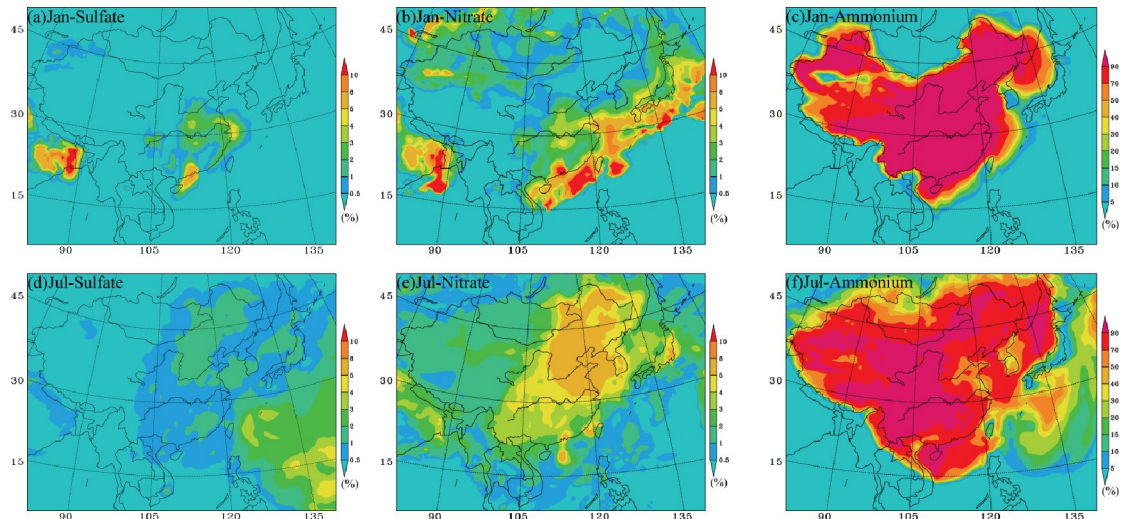


Figure R1 The horizontal distributions of the contribution percentage of NH_3 emissions to sulfate, nitrate and ammonium mass burden (%) in January and July.

Minor points:

1. In Figure 6 and Figure 7, it should be the horizontal distributions in January, April, July, and October.
2. In Line 226, it should be “Since NH_3 concerns mainly with secondary inorganic aerosols (SNA): sulfate, nitrate, and ammonium formation”.
3. In line 269, what is “TA NH_3 emission”?
4. In Line 833, should is it “The regional percent (%) of Tagr NH_3 contribution”?

R: Thanks for the comments. All error points were modified.

112 **RC2:**

113 The NH₃ emissions from agricultural activities in China, which is one of the largest agricultural
114 countries in the world, significantly affect regional air quality and horizontal visibility. In this study, the
115 contributions of NH₃ from multiple agricultural emissions to aerosols were calculated using the RAMS-
116 CMAQ-ISAM system; it allowed to trace the transport and chemical reactions of NH₃ from fertilizer and
117 husbandry emissions sectors to quantitatively estimate the contribution of agricultural NH₃ emissions to
118 the PM_{2.5} mass concentration in China. As input was used the high-resolution PKUNH₃ emissions
119 inventory, which was complemented with MIX Asian, REAS and GFED data; different meteorological
120 factors were used to capture the formation processes and transport of secondary aerosols. For model
121 evaluation, several observation data were compared with the simulation results for both meteorological
122 parameters and SO₂, NO₂, and PM_{2.5}.

123 Major points. Suggestion: the “Results and discussions” section should be extended by providing
124 explanations on different aspects.

125 *1) How the emissions input influences the changes in concentrations patterns? Please discuss the*
126 *seasonal variation in emissions for the months of January, April, July and October.*

127 R: Thanks for this comment. The horizontal distribution, budget, and seasonal variations of PKU-NH₃
128 emission inventory have been shown in the papers published by Prof. Song’s research team (Kang et al.,
129 ACP, 2016; Liu et al, PNAS, 2019). Therefore, this information will not be displayed here again. However,
130 we try to extract the emission data from PKU-NH₃ inventory, and added Figure A5 which provided the
131 regional average emission flux of each sectors (g/s/grid) over several major regions in January, April, July
132 and October. It can be seen that the emission flux was higher in summer and lower in winter. The strongest
133 emission flux mainly appeared in BTH, SDP and CNC, and the values in YRD, SCB and NEC was higher,
134 too. These features generally followed the distribution pattern of NH₃ mass concentration as shown in
135 Figure 3. We have added the statement in Appendix A. Please check if it is appropriate.

136
137 *2) Identify, which of the agricultural sub-sectors, i.e., fertiliser, husbandry, farmland ecosystems,*
138 *livestock waste, crop residue burning, and excrement waste from rural populations, are contributing most*
139 *to the seasonal changes.*

140 R: Thanks for this comment. Furthermore, the contribution percent of each sector emission fluxes were
141 calculated and shown in Figure A6. It can be seen that the highest proportion was contributed by husbandry,

142 followed by the contribution of fertilizer. The total percent of husbandry and fertilizer was relatively higher
143 in spring and summer, but lower in winter (brodly higher than 60% at least). In general, the emission from
144 husbandry and fertilizer should be the major contributor to NH_3 . In addition, the contribution of other sector,
145 including industry, residential and transport, was also obvious. The discussion has been added to the paper
146 (Appendix A). Please check if it is appropriate.

147
148 *3) Emphasis the influence of meteorological conditions.*

149 R: Thanks for this comment. We added the monthly horizontal distribution of the surface wind field
150 in Figure 4, and modified related discussion (Line 225-227). Please check if it is suitable.

151
152 *4) How this tool could support policy makers in designing the $\text{PM}_{2.5}$ emissions mitigation strategy in
153 China.*

154 R: Thanks for this comment. The model system can be used to capture the source contribution features
155 over the regions we concerned. The emission sectors and transport features can be obtained quantitatively
156 based on the simulation results. Then, we can determine whether the control strategy is needed, and how
157 much emission flux should be reduced. This is a useful tool for $\text{PM}_{2.5}$ because most of the $\text{PM}_{2.5}$ components
158 are secondary species, which is hard to capture the source contribution features due to the strong nonlinear
159 effect. Therefore, the model system should be helpful to make the $\text{PM}_{2.5}$ emission control policy in China.
160 However, the specific policies depend on more detail information in different regions (such as natural
161 background, economic conditions, industrial structure, etc.), not only produced by the model simulation
162 results.

163
164 *5) Explain why “the influence of NH_3 would enhance with the decreasing of ambient NH_3 mass
165 concentration”; provide directions for further research on this topic.*

166 R: Thanks for this comment. This feature was deeply discussed by Wang et al. (2011; Impact
167 Assessment of Ammonia Emissions on Inorganic Aerosols in East China Using Response Surface
168 Modeling Technique). The results of RSM (Response Surface Modeling) in their study shows that the
169 change of NO_3^- mass concentration is very sensitive to the emission level of NH_4^+ and performs as
170 nonlinear relationship. The reduction of NH_3 emissions can play a very significant role in reducing the mass
171 concentration of NO_3^- under NH_3 -poor condition. However, there will be excess NH_3 in the atmosphere

172 under NH₃-rich condition, and these excess NH₃ could neutralizes more nitric acid even in the case of
173 emission reduction. Thus, the emission reduction effect is not significant under NH₃-rich condition. In
174 addition, the SO₂ will compete for NH₃ and prevent the generation of NH₄NO₃ under NH₃-poor condition
175 because the reaction between H₂SO₄ and NH₃ takes precedence over the one between HNO₃ and NH₃.
176 Oppositely, SO₂ should be benefit for the formation of NO₃⁻ (especially in summer) under NH₃-rich
177 condition according to the calculation of Wang et al. (2011). This should be a reason why the effect of NH₃
178 emission control is not obvious in the case of NH₃-rich condition as well.

179
180
181 Minor points:

182 For the regions in China for which the findings are discussed – spell them out (e.g. “NEC”). Figure 6
183 – add to the caption “April and October”. What is T in Table 2 - “of T contribution”. What is TA, Page 9,
184 line 269 - “10% TA NH₃ emission”.

185 R: Thanks for the comments. All error points were modified.

186
187
188
189
190
191
192
193
194
195
196
197

198 **Numerical analysis of agricultural emissions impacts on PM_{2.5} in China using a high-**
199 **resolution ammonia emission inventory**

200 Xiao Han^{1,2}, Lingyun Zhu⁵, Mingxu Liu⁴, Yu Song⁴, Meigen Zhang^{1,2,3},

201 ¹*State Key Laboratory of Atmospheric Boundary Layer Physics and Atmospheric Chemistry, Institute of*
202 *Atmospheric Physics, Chinese Academy of Sciences, Beijing 100029, China*

203 ²*College of Earth and Planetary Sciences, University of Chinese Academy of Sciences, Beijing 100049,*
204 *China*

205 ³*Center for Excellence in Urban Atmospheric Environment, Institute of Urban Environment, Chinese*
206 *Academy of Sciences, Xiamen 361021, China*

207 ⁴*State Key Joint Laboratory of Environmental Simulation and Pollution Control, Department of*
208 *Environmental Science, Peking University, Beijing 100871, China.*

209 ⁵*Shanxi Province Institute of Meteorological Sciences, Taiyuan 030002, China*

210

211

212

213

214

215

216

217

218

219

220

221

222

223

224

225

226

227 **Abstract**

228 China is one of the largest agriculture country in the world. The NH₃ emission from agriculture activities
229 are significantly affects the regional air quality and horizontal visibility in China. To reliably estimate the
230 agriculture NH₃ influence, a high-resolution agriculture NH₃ emission inventory compiled on 1km × 1km
231 horizontal resolution was applied for calculating the NH₃ mass burden in China. The key parameter
232 emission factors of this inventory was enhanced by considering many native experiment results, and the
233 activity data of spatial and temporal information were updated by the statistic data in 2015. Not only
234 fertilizer and husbandry, but also farmland ecosystems, livestock waste, crop residue burning, fuel wood
235 combustion, and other NH₃ emission sources were included in this inventory. Furthermore, a source
236 apportionment tool, ISAM (Integrated Source Apportionment Method), coupled with the air quality
237 modeling system RAMS-CMAQ (Regional Atmospheric Modeling System and Community Multiscale Air
238 Quality), was applied to capture the contribution of NH₃ emitted from total agriculture (Tagr) in China. The
239 aerosol mass concentration in 2015 was simulated and the results showed that the high mass concentration
240 of NH₃ which exceeded 10 μg m⁻³ mainly appeared in the North China Plain (NCP), Central China (CNC),
241 Yangtz River Delta (YRD), and Sichan Basin (SCB), and the annually average contribution of Tagr NH₃ to
242 PM_{2.5} mass burden was 14-22% in China. Specific to the PM_{2.5} components, Tagr NH₃ provided major
243 contribution to the ammonium formation (87.6%), but tiny contribution to the sulfate (2.2%). In addition,
244 several brute-force sensitive tests were conducted to estimate the impact of Tagr NH₃ emission reduction
245 on PM_{2.5} mass burden. Compared with the result of ISAM, it was found that even though the Tagr NH₃
246 only provided 10.1% contribution to nitrate under current emission scenario, the reduction of nitrate could
247 reach 95.8% upon removal of the Tagr NH₃ emission. The main reason of this deviation should be that the
248 NH₃ contribution to nitrate should be small under "rich NH₃" and large under "poor NH₃" environment.
249 Thus, the influence of NH₃ on nitrate formation would enhance with the decreasing of ambient NH₃ mass
250 concentration.

251

252

253

254

255

256

1. Introduction

Ammonia (NH_3) is an important pollution species which principal neutralizing agent for the acid aerosols, SO_4^{2-} and NO_3^- formed from the SO_2 and NO_x (Chang, 1989; McMurry et al.; 1983). In addition, NH_3 also influences the rate of particle nucleation (Ball et al.; 1999; Kulmala et al.; 2002) and enhances secondary organic aerosols (SOA) yields (Babar et al.; 2017). The widespread haze events have frequently occurred in most regions of eastern China in recent years, and several studies have reported that the secondary inorganic salts, including sulfate, nitrate, and ammonium, were the majorities of the total aerosols in the urban and rural regions (Tao et al.; 2014; Wang et al.; 2016; Zhang et al.; 2012; Lai et al.; 2016; Zhang et al.; 2018). Therefore, besides the heavy emissions of SO_2 and NO_2 , NH_3 emissions from the agriculture activities are also non-negligible.

China is one of the largest agriculture country in the world. Even though a decrease appeared from 2006 to 2012, the annual emission budget of NH_3 which reached 9.7-12 Tg (Kang et al.; 2016; Xu et al.; 2016; Zhou et al.; 2015) was still huge and leads to high NH_3 ambient concentration. This massive NH_3 significantly affects the regional air quality and horizontal visibility. Firstly, the major $\text{PM}_{2.5}$ components, $(\text{NH}_4)_2\text{SO}_4$, $(\text{NH}_4)_3\text{H}(\text{SO}_4)_2$, NH_4HSO_4 , and NH_4NO_3 were partially or fully yielded from neutralizing H_2SO_4 and HNO_3 by the NH_3 reacts (Tanner et al.; 1981; Brost et al.; 1988; Quan et al.; 2014; Zhao et al.; 2013; Zhang et al.; 2014). Studies also showed that NH_3 improves the H_2SO_4 nucleation by 1-10 times (Benson et al.; 2011), and provides sufficient new particle to alter the number and size distributions. Thus, the NH_3 and its secondary product NH_4^+ play an important role in the formation of air pollution and haze days. Some research showed that about 80% of total anthropogenic NH_3 emissions derived from the agriculture sources, and the livestock manure provided more contributions than that of the synthetic fertilizer (Kang et al. 2016; Zhou et al.; 2016). The Chinese government has taken several control strategies to reduce the particle pollutions and their precursors, such as the catalytic reduction systems in the power sector (Xia et al.; 2016), measures to change coal to gas for residents' life and heating (Ren et al.; 2014), etc. Related observations have shown that the mass burden of SO_2 and NO_x have distinctly decreased in recent year (De Foy et al.; 2016; Wang et al.; 2015; Zheng et al.; 2018). However, there was no specific measures for agriculture NH_3 emission control have been implemented until now and the total agriculture NH_3 emission budget was not obviously changed from 2010 to 2017 (Zheng et al.; 2018).

In addition, an accurate information of agriculture NH_3 emission is also important for estimating the NH_3 mass burden and its environmental effect. There were several studies focusing on NH_3 emissions from

287 agricultural activities in China or East Asia. REAS (Regional Emission inventory in Asia) version 2
288 established an anthropogenic emission inventory which includes the source of agricultural NH₃ (fertilizer
289 application and livestock) (Kurokawa et al.; 2013). This inventory targeting years from 2000 to 2008 has
290 0.25×0.25 degree spatial resolution with monthly variation. MASAGE_NH₃ (Magnitude and Seasonality
291 of Agricultural Emissions model for NH₃) developed a bottom-up NH₃ emission inventories by using the
292 adjoint of the GEOS-Chem chemical transport model (Paulot et al.; 2014). The network data for NH₄⁺ wet
293 deposition fluxes from 2005-2008 were inversed to optimize the NH₃ emission in China in this inventory.
294 Fu et al. (2015) used CMAQ model coupled to an agro-ecosystem to estimate the NH₃ emissions with high
295 spatial and temporal resolution in 2011, which could obtain hourly emission features by online model
296 calculation. These NH₃ emission inventory provided very useful datasets for understanding the distribution
297 features of NH₃ mass burden in China. However, with the migration of population, economic growth, and
298 increasing of agricultural products consumption, the spatial distribution and strength of agriculture NH₃
299 emission was significantly changed in China during last decade (Xu et al.; 2017), so that a reliable emission
300 information based on recent year is also necessary for estimating the NH₃ mass burden.

301 Previous studies have investigated the influence of NH₃ emission to aerosol loading in several typical
302 areas of China. Wu et al. (2008) conducted sensitivity studies to assess the impact of the livestock NH₃
303 emissions on PM_{2.5} mass concentration in North China by using MM5/CMAQ modeling system. The results
304 showed that the livestock NH₃ provided >20% contributions to nitrate and ammonium, but provided quite
305 small contribution to sulfate. Wang et al. (2011) used the response surface modeling technique to estimate
306 the NH₃ emission contribution in the East China, and found that the total NH₃ emission contributed 8-11%
307 to PM_{2.5} concentration, and the nonlinear effects were significant while the transition between NH₃ rich and
308 poor conditions. Fu et al. (2017) and Zhao et al. (2017) also investigated the impact of NH₃ emission on
309 PM_{2.5} in East China and Hai River Basin. However, the related research was still less and mainly focused
310 on the local regions, and most of them generally used the brute-force sensitivity method to estimate the
311 NH₃ impact based on chemistry model, which reflect the particle concentration change with emission
312 reduction (Koo et al.; 2009).

313 A comprehensive high-resolution NH₃ emission inventory PKU-NH₃ based on the year 2015 is applied
314 in this study to capture the agriculture NH₃ mass concentration in China, and the contribution to PM_{2.5}
315 particle was estimated by an air quality modeling system RAMS-CMAQ coupled with the online source
316 tagged module ISAM. Compared with previous studies, this high-resolution agriculture NH₃ emission

317 inventory is more accurate and reflects the latest spatial and temporal distribution features (Liu et al.; 2019).
318 The major trace gases and aerosol species in 2015 were simulated by the modeling system and evaluated
319 by several observation data. The contribution to the pollutant concentrations can be tagged and quantified
320 by RAMS-CMAQ-ISAM under current scenario (Wang et al.; 2009). Then, several brute-force sensitivity
321 tests were conducted to estimate the effect of reducing agriculture NH₃ emission on the PM_{2.5} mass burden
322 as well. The results from the source apportionment simulation and brute-force sensitivity tests in January,
323 April, July, and October were present, and the detail features over seven major populated areas (as shown
324 in Figure 1) of China were mainly discussed.

325

326 **2. Methodology**

327 The emission inventory was described as follow. Firstly, the NH₃ emission data in China was provided
328 by the PKU-NH₃ emission inventory (Kang et al.; 2016; Zhang et al.; 2018). This inventory was developed
329 on the basis of previous studies (Huang et al.; 2012) and improved the horizontal resolution and accuracy.
330 It compiled on 1km×1km horizontal resolution with monthly based statistic data in 2015. One of the most
331 uncertainty parameter the emission factors applied in this inventory was enhanced by considering as many
332 native experiment results as possible with ambient temperature, soil acidity, and other factors change. In
333 addition, this inventory not only includes the fertilizer and husbandry emission from agriculture activities,
334 but also collects the emission data of farmland ecosystems, livestock waste, biomass burning (forest and
335 grassland fires, crop residue burning, and fuel wood combustion), and other sources (excrement waste from
336 rural populations, the chemical industry, waste disposal, NH₃ escape from thermal power plants, and traffic
337 sources). Secondly, the anthropogenic emission of primary aerosols and the precursors were obtained from
338 the MIX Asian emission inventory (base year 2012) prepared by the Model Inter-Comparison Study for
339 Asia (MICS-ASIA III) (Lu et al.; 2011; Lei et al.; 2011). The anthropogenic emission sources of SO₂, NO_x,
340 volatile organic compounds (VOCs), black carbon (BC), organic carbon (OC), primary PM_{2.5}, and PM₁₀
341 were obtained from the monthly-based MIX inventory with 0.25°×0.25° spatial resolution. The REAS
342 (Regional Emission Inventory in Asia; Version 2; Kurokawa et al.; 2013) and GFED (Global Fire Emissions
343 Database; Version 3; van der Werf et al.; 2010) were used to provide the VOCs, nitrogen oxides from flight
344 exhaust, lighting, paint, wildfires, savanna burning, and slash-and-burn agriculture.

345 The modeling system RAMS-CMAQ was applied to simulate the transformation and transport of
346 pollutants in atmosphere. The regional air quality model CMAQ (version 5.0.2) released by US

347 Environmental Protection Agency (Eder et al.; 2009; Mathur et al.; 2008) was the major component of the
348 RAMS-CMAQ modeling system. In this model, The CB05 (version CB05tucl) chemical mechanism
349 (Whitten, 2010) was used to treat the gas-phase chemical mechanism. The simulation of O₃ in urban plumes,
350 which could impacts the NO_x chemical transformation and fine particle mass predictions, was updated in
351 this version for obtaining more reasonable results. The sixth-generation model CMAQ aerosol model
352 (AERO6) which added 9 new PM_{2.5} species and updated the secondary organic aerosol (SOA) yield
353 parametrization and primary organic aerosol (POA) aging processes was used to simulate the formation
354 and dynamic processes of aerosols. ISORROPIA model (version 2.1) (Fountoukis and Nenes, 2007) was
355 used to describe the thermodynamic equilibrium of gas-particle transformation. The highly versatile
356 numerical model RAMS which can well capture the boundary layer and the underlying surface was applied
357 to provide the meteorological fields for CMAQ (Cotton et al.; 2003). The European Centre for Medium-
358 Range Weather Forecasts reanalysis datasets (1°×1° spatial resolution) were used to supply the background
359 fields and sea surface temperatures. The model domain (Figure 1) is 6654 km × 5440 km with 64 km² fixed
360 grid cells, and uses a rotated polar stereographic map projection covered the whole mainland of China and
361 its surrounding regions. The model has 15 vertical layers and half of them are located in the lowest 2 km to
362 provide more precise simulation of the atmospheric boundary layer.

363 The ISAM is a flexible and efficient on-line source apportionment implementation which was used to
364 track multiple pollutants emitted from different geographic regions and source types. Compared with its
365 previous version TSSA (Tagged Species Source Apportionment), the processes of tracking tagged tracer
366 transport and precursor reaction were optimized for balancing the computational requirements and reliable
367 representation of the physical and chemical evolution. In order to reduce the nonlinear effect during phase
368 transformation and relative chemical interactions, a standalone subroutine “wrapper” approach was applied
369 in ISAM to apportion the secondary PM species and their precursor gases during the thermodynamic
370 equilibrium simulation; a hybrid approach which employing the LU decomposition triangular matrices
371 (Yang et al.; 1997) was developed for describing the gas-phase chemical interactions as well. In this study,
372 ISAM was coupled into RAMS-CMAQ and set to trace the transport and chemical reactions of the NH₃
373 from fertilizer and husbandry emission sectors for quantitatively estimating the contribution of agriculture
374 NH₃ emission to the PM_{2.5} mass concentration in China.

375

376 **3. Model evaluation**

377 In order to evaluation the model performances, several observation data are used to compared with the
378 simulation results. The meteorological factors are important to capture the formation processes and
379 transport of secondary aerosols. Thus, in this paper, the observed meteorological data from surface stations
380 of the Chinese National Meteorological Center are collected to evaluate the performance of the model. The
381 detail information is described in Appendix A. Furthermore, the observed SO₂, NO₂, and PM_{2.5} released
382 from the Ministry of Environmental Protection of China were applied to evaluate the modeled mass
383 concentration of these pollutants. The hourly observation data in January, April, July and October at 6
384 stations that located in Beijing, Jinan, Shijiazhuang, Nanjing, Guangzhou and Zhengzhou were collected in
385 this study. The scatter plots of comparison are shown in Figure 2, and the statistical parameters between the
386 observations and simulations are listed in Table 1-3. It can be seen that most of the scatter points broadly
387 gather around the 1:1 solid line. Most of the correlation coefficients in Table 1-3 are higher than 0.5, which
388 indicates that the model can capture the regional variation features of measurements. The standard
389 deviations between the observation and simulation were similar in most cases as well. The simulation
390 results performed better in winter than that in summer because the diffusion condition was strong and the
391 mass concentration changed noticeably during summer time. The modeled PM_{2.5} generally performed well
392 due to relatively high correlation coefficients. The obvious deviation of the modeled mean, which was
393 higher than that of the observation, was between the observed and modeled SO₂. The emission of SO₂
394 reduced rapidly because of the control measures from 2013 in China. However, the emission inventory may
395 not reflect this feature and slightly overestimated the mass burden.

396 The horizontal distributions of modeled monthly NH₃ mass concentration in January, April, July, and
397 October in 2015 are shown in Figure 3. Pan et al. (2018) provided the distributions of satellite NH₃ total
398 column distribution and the surface NH₃ concentrations at several observation sites in their Figure 1. As
399 shown from their results, the highest mass burden mainly concentrated in North China Plain (NCP), Central
400 China (CNC), Yangtz River Delta (YRD), and Sichan Basin (SCB). The simulation results in this study
401 broadly reflected these distribution features. The values of NH₃ concentrations in these regions could reach
402 10-25 μg m³ in Pan et al. (2018), which also coincided well with the simulation results. However, some
403 obvious deviation appeared in the areas of east part of Gansu province. The modeled NH₃ in these regions
404 by this study was slightly higher than those of the observations in Pan et al. (2018). Zhang et al. (2018) also
405 showed the NH₃ mass concentration in four seasons over China from simulation (horizontal distribution)
406 and ground-based measurements (point values) in their Figure 9. Besides the regions maintained in Pan et

407 al. (2018), the high mass burden of NH_3 also appeared in the Northeast China (NEC) as shown by both
408 simulation and observation in Zhang et al. (2018). Generally, this distribution feature should be reasonable
409 because the Three River Plain located in NEC is an important agriculture base of China, and the NH_3
410 emission in this region can be strong during spring and summer. The simulation results in this study also
411 followed the seasonal variation feature of NH_3 mass burden as shown in Zhang et al. (2018), which was
412 higher in summer and lower in winter, and the magnitude was also close with each other. Thus, it can be
413 seen that the modeled NH_3 concentration by RAMS-CMAQ was reliable and can be applied for the analysis
414 in this study.

415

416 **4. Results and discussions**

417 The horizontal distributions of modeled monthly $\text{PM}_{2.5}$ mass concentration in January, April, July, and
418 October in 2015 was shown in Figure 4. The surface wind field was also shown in Figure 4. Over the east
419 part of China, the heavy $\text{PM}_{2.5}$ pollution happened in January and the relatively better air quality appeared
420 in July. The large $\text{PM}_{2.5}$ mass burden exceeded $200 \mu\text{g m}^{-3}$ in January mainly concentrated in the NCP, the
421 Yangtze River Valley of CNC, and SCB, which broadly coincided with the regions covered by high mass
422 burden of NH_3 as shown in Figure 3. **It can be seen that the wind speed in the regions mentioned above was**
423 **relatively weak, implying that the diffusion condition was not good, and more aerosol can be trapped in**
424 **these region. In addition, the $\text{PM}_{2.5}$ mass burden ($50\text{-}150 \mu\text{g m}^{-3}$) was obviously lower than other months**
425 **in July. Since the NH_3 emission mainly concerns with the secondary inorganic aerosols (SNA): sulfate,**
426 **nitrate, and ammonium formation,** the analysis hereafter will mainly focus on the SNA. Figure 5 present
427 the modeled monthly SNA mass concentration in January, April, July, and October in 2015. The mass
428 loading of SNA generally provided 40-60% to the total $\text{PM}_{2.5}$ in the east part of China, which was
429 comparable with previous studies (Cao et al.; 2017; Chen et al.; 2016; Lai et al.; 2016; Wang et al.; 2016).
430 The distribution pattern and seasonal variation of SNA also followed the features of $\text{PM}_{2.5}$, and the high
431 mass concentration of SNA could exceed $100 \mu\text{g m}^{-3}$ in January.

432 Then, the contributions of NH_3 from the multiple agriculture emission (includes fertilizer, husbandry,
433 farmland ecosystems, livestock waste, crop residue burning, and excrement waste from rural populations)
434 to aerosols were calculated using RAMS-CMAQ-ISAM; the monthly average contribution percentage of
435 total agriculture activities (Tagr) in January, April, July, and October are shown in Figure 6. Generally, the
436 Tagr NH_3 provided 30-50% contribution in January and October, and 20-40% contribution in April and

437 July to the SNA over the most part of east China. The relatively lower value mainly appeared in April.

438 The regional average percent of Tagr contribution to sulfate, nitrate, ammonium, SNA, and PM_{2.5} are
439 shown in Table 4. As shown in this table, the annually average Tagr NH₃ provided major contribution which
440 reached about 90% to ammonium and relatively small contribution which was 5-10% to nitrate mass burden.
441 However, the contribution to sulfate was tiny and the main reason should be that there are various ways of
442 sulfate formation from SO₂ besides neutralized by NH₃, such as oxidized by H₂O₂, O₃, or peroxyacetic
443 acid. The seasonal variation of ammonium was obvious: it could higher than 99% in January but lower than
444 70% in July. Most of the difference as shown in Table 4 could exceeded 10% because the NH₃ emitted from
445 other sources (anthropogenic and natural sources) was significant in these regions during summer time. The
446 annually average Tagr NH₃ provided 20-40% contribution to the SNA mass concentration, and the
447 contributions in January were larger than that in July as well. The seasonal variation and spatial features of
448 Tagr NH₃ contribution to PM_{2.5} mass concentration were similar with the features of SNA, and generally
449 provided approximate 14-22% contribution to the total PM_{2.5} mass concentration in these places. On the
450 other hand, it can be seen that the annual contribution in China were higher than those of the contribution
451 in the regions mentioned above. This feature indicated that the Tagr NH₃ provided more contribution than
452 other sources over the regions with weaker anthropogenic activities.

453 In addition, the brute-force method (zero-out sensitivity test) which can capture the effect of emissions
454 change on aerosol mass burden was applied to investigate the impact of the removal of Tagr NH₃ emission.
455 Unlike the on-line source apportionment, the brute-force method mainly reflects the disparity of chemical
456 balance caused by the emissions change, which could significantly alter the secondary pollutant formation.
457 Several sensitivity tests were conducted and the results are shown in Figure 7 and Table 5. Figure 7 presents
458 the mass burden variation of SNA associated with the Tagr NH₃ removal. From Figure 7, it can be seen that
459 the reduction pattern and seasonal variation of the aerosol were broadly followed those of their mass burden.
460 The significant reduction of SNA mainly appeared in the high concentration regions, and generally
461 exceeded 25 $\mu\text{g m}^{-3}$. Table 5 shows the percentage of the variation of sulfate, nitrate, ammonium, SNA, and
462 PM_{2.5}. Compared with Table 4, it can be found that the variation percent of SNA and PM_{2.5} which reached
463 30-60% and 24-42%, respectively, were about two times higher than those of the contribution percent, and
464 this significant distinction was mainly caused by the variation of nitrate: the contribution of Tagr NH₃ to
465 nitrate was generally below 10% as shown in Table 4, but the reduction of nitrate associated with removing
466 **Tagr NH₃ emission** could exceed 90% as shown in Table 5. This difference between the results of ISAM

467 and brute-force was expected as a result of high nonlinearity in the NO_x chemistry. The nitrate formation
468 could become more sensitive when the “rich NH_3 ” environment shifts to “poor NH_3 ” environment, which
469 means the decrease of nitrate mass burden would accelerate with the NH_3 emission reduction. Therefore, it
470 can be deduced that the contribution of NH_3 to nitrate should be significantly lower under “rich NH_3 ”
471 environment than that under “poor NH_3 ” environment. Similar phenomenon was also reported by some
472 previous study (Wang et al.; 2011; Xu et al.; 2016). To prove this point, more brute-force sensitivity tests
473 were conducted. The variation of sulfate, nitrate, ammonium, and SNA mass burden associated with the
474 reduction of NH_3 emission (80%, 50%, 40%, 30%, 20%, and 10% Tagr NH_3 emission, respectively) was
475 shown in Figure 8. It can be seen that the decline of nitrate mass concentration was more rapid than that of
476 ammonium, and the trend became slightly faster with the reduction of NH_3 emission (signifying from “rich
477 NH_3 ” to “poor NH_3 ”) in the most regions. The acceleration of nitrate mass burden decline was more
478 significant in the regions with strong NH_3 emission. Furthermore, this acceleration stopped while 20% NH_3
479 emission remained as shown in Figure 8.

480

481 **5. Conclusions**

482 The emission budget of agriculture NH_3 was huge and played an important role on the regional particle
483 pollution in China. As a precursor of the secondary aerosol, reasonably estimate the nonlinear processes of
484 secondary aerosol formation should be the key point for capturing the contribution of NH_3 to particle
485 pollution. In this study, the air quality modeling system RAMS-CMAQ was applied to simulate spatial-
486 temporal distribution of trace gas and aerosols in 2015. In addition, the PKU- NH_3 emission inventory which
487 compiled on $1\text{km} \times 1\text{km}$ horizontal resolution with monthly based data was applied to accurately capture
488 the agriculture NH_3 emission features in China. Then, the source apportionment module ISAM was coupled
489 into this modeling system to quantitatively estimate the contribution of agriculture NH_3 to $\text{PM}_{2.5}$ mass
490 burden. The brute-force sensitivity tests were also conducted for discussing the impact of the agriculture
491 NH_3 emission reduction. The meteorological factors and mass concentration of NH_3 , SO_2 , NO_2 , and $\text{PM}_{2.5}$
492 from simulation were evaluated and showed well agreement with the observation data. Some interesting
493 results were explored and summarized as follow:

494 (1) The high mass burden of NH_3 could exceeded $10 \mu\text{g m}^{-3}$, and mainly appeared in the NCP, CNC,
495 YRD, and SCB. These regions were highly coincidence with the regions that heavy particle pollution
496 covered in China. Therefore, it can be deduced that the influence of agriculture NH_3 on the $\text{PM}_{2.5}$ mass

497 concentration should be significant.

498 (2) The results from ISAM simulation shows that the Tagr NH₃ provided 17-23% and 15-22%
499 contribution to the PM_{2.5} in January and July, respectively, in the most part of east China, and the largest
500 annual average contribution appeared in CNC (17.5%). Specific to the SNA components, the annually and
501 regional average contribution of Tagr NH₃ to ammonium, nitrate, sulfate was 87.6%, 10.1%, and 2.2% in
502 China. The agriculture NH₃ emission provided major contribution to the ammonium formation, but tiny
503 contribution to the sulfate due to the various other ways of sulfate formation.

504 (3) The brute-force sensitive test could reflect the effect of changing Tagr NH₃ emission on PM_{2.5} mass
505 burden. The results indicated that the reduction percent of PM_{2.5} mass burden due to removal Tagr NH₃
506 emission could reach 24-42% in the most part of east China, which was approximately two times higher
507 than the contribution. The reduction percent of nitrate that reached exceed 90% was the main reason caused
508 this significant different. In addition, the further analysis proved that the ambient NH₃ mass burden could
509 obviously affects its contribution to the SNA formation: the NH₃ contribution to nitrate should be lower
510 under "rich NH₃" and higher under "poor NH₃". Therefore, the influence of NH₃ would enhance with the
511 decreasing of ambient NH₃ mass concentration.

512 It is suggested that the NH₃ influence on the PM_{2.5} mass burden are complex because of the
513 nonlinearity of secondary aerosol formation. Significantly deviation exists between the results from ISAM
514 and brute-force method, so that these two kinds of results should be distinguished and applied to explain
515 different issues: the contribution under current scenario and the effect due to emission reduction,
516 respectively. The modeling system is a versatile tool allows us to investigate these valuable information for
517 choosing more efficient strategies of reducing the impact of agriculture NH₃ and improving air quality.

518 **Acknowledgments**

519 This work was supported by the Strategic Priority Research Program of the Chinese Academy of
520 Sciences (XDA19040204), and the National Natural Science Foundation of China (41830109).

521
522
523
524
525
526

527 **Appendix A**

528 The daily average temperature, relative humidity, wind speed and maximum wind direction in January,
529 April, July and October 2015 were compared with the surface shared data from the Chinese National
530 Meteorological Center (<http://data.cma.cn/>) in 9 stations. The comparison results are shown in Figure A1-
531 A4. These stations are located in the East China where the high NH₃ emission regions. Generally, the
532 modeled temperature was in good agreement with the observed data, and can reflect the large fluctuation
533 and seasonal variation of relative humidity as well, except that some of the extreme high or low values
534 appeared abruptly. As shown in Figure A3, most of the daily average wind speed was lower than 3 m s⁻¹ at
535 Zhengzhou, Miyun, Tianjin and Baoding station (all located in the North China Plain), which means the
536 diffusion condition was not good due to the stable weather. Otherwise, the relatively strong wind appeared
537 at Nanjing, Chaoyang, Nanning and Jinan. The modeled wind speed generally reproduced all these features.
538 The direct comparison between observed and modeled wind direction which can be easily influenced by
539 the surrounding surface features is difficult. Nevertheless, the prevailing wind direction in different seasons
540 can be captured by the simulation results for all stations.

541 In addition, Figure A5 present the regional average NH₃ emission flux (g/s/grid) of different sectors,
542 including fertilizer, Husbandry, Biomass burning, Farmland ecosystems, Waste disposal, and other sectors,
543 over each regions in January, April, July and October. Furthermore, the percent (%) of each NH₃ emission
544 sector was shown in Figure A6. All the information was obtained from the PKU-NH₃ emission inventory
545 directly. It can be seen that the emission flux was higher in summer and lower in winter. The strongest
546 emission flux mainly appeared in BTH, SDP and CNC. The distribution pattern of NH₃ mass concentration

547 These features generally followed the distribution pattern of NH₃ mass concentration as shown in
548 Figure 3. On the other hand, the major proportion was provided by husbandry and fertilizer, and relatively
549 higher in spring and summer.

550
551
552
553
554
555
556

Reference

557

- 558 Babar, Z. B.; Park, J.; Lim, H. Influence of NH₃ on secondary organic aerosols from the ozonolysis and photooxidation of
559 a -pinene in a flow reactor. *Atmos. Environ.* 2017, 164, 71-84, DOI: 10.1016/j.atmosenv.2017.05.034
- 560 Ball, S. M.; Hanson, D. R.; Eisele, F. L.; McMurry, P. H. Laboratory studies of particle nucleation: Initial results for H₂SO₄,
561 H₂O, and NH₃ vapors. *J. Geophys. Res.* 1999, 104, 23709-23718, DOI: 10.1029/1999JD900411
- 562 Benson, D. R.; Yu, J. H.; Markovich, A.; Lee, S. H. Ternary homogeneous nucleation of H₂SO₄, NH₃, and H₂O under
563 conditions relevant to the lower troposphere. *Atmos. Chem. Phys.* 2011, 11, 4755-4766, DOI: 10.5194/acp-11-4755-
564 2011
- 565 Brost, R. A.; Delany, A. C.; Huebert, B. J. Numerical modeling of concentrations and fluxes of HNO₃, NH₃, and NH₄NO₃
566 near the ground. *J. Geophys. Res.* 1988, 93, 7137-7152, DOI: 10.1029/JD093iD06p07137
- 567 Cao, Z.; Zhou, X.; Ma, Y.; Wang, L.; Wu, R.; Chen, B.; Wang, W. The concentrations, formations, relationships and
568 modeling of sulfate, nitrate and ammonium (SNA) aerosols over China. *Aerosol Air Qual. Res.* 2017, 17, 84-97, DOI:
569 10.4209/aaqr.2016.01.0020
- 570 Chen, Y.; Schleicher, N.; Cen, K.; Liu, X.; Yu, Y.; Zibat, V.; Dietze, V.; Fricker, M.; Kaminski, U.; Chen, Y.; Chai, F.; Norra,
571 S. Evaluation of impact factors on PM_{2.5} based on long-term chemical components analyses in the megacity Beijing,
572 China. *Chemosphere* 2016, 155, 234-242, DOI: 10.1016/j.chemosphere.2016.04.052
- 573 Chang, J. The role of H₂O and NH₃ on the formation of NH₄NO₃ aerosol particles and De-NO_x under the corona discharge
574 treatment of combustion flue gases. *J. Aerosol Sci.* 1989, 20, 1087-1090, DOI: 10.1016/0021-8502(89)90768-4
- 575 Cotton, W.; Pielke, R.; Walko, G.; Liston, G.; Tremback, C.; Jiang, H.; McAnelly, R.; Harrington, J.; Nicholls, M.; Carrio,
576 G.; McFadden, J. RAMS 2001: current status and future directions, *Meteorol. Atmos. Phys.* 2003, 82, 5-29, DOI:
577 DeFoy, B.; Lu, Z.; and Streets, D. G. Satellite NO₂ retrievals suggest China has exceeded its NO_x reduction goals from the
578 twelfth five-year plan. *Sci. Rep.* 2016, 6, 35912, DOI: 10.1007/s00703-001-0584-9
- 579 Eder, B.; Yu S. A performance evaluation of the 2004 release of Models-3 CMAQ. *Atmos. Environ.* 2006, 40, 4811-4824,
580 DOI: 10.1016/j.atmosenv.2005.08.045
- 581 Fountoukis, C.; Nenes, A. ISORROPIA II: a computationally efficient thermodynamic equilibrium model for K⁺-Ca²⁺-
582 Mg²⁺-NH₄⁺-Na⁺-SO₄²⁻-NO₃⁻-Cl⁻-H₂O aerosols. *Atmos. Chem. Phys.* 2007, 7, 4639-4659, DOI: 10.5194/acp-7-4639-
583 2007
- 584 Fu, X.; Wang, S.; Xing, J.; Zhang, X.; Wang, T.; Hao, J. Increasing Ammonia Concentrations Reduce the Effectiveness of
585 Particle Pollution Control Achieved via SO₂ and NO_x Emissions Reduction in East China. *Environ. Sci. Technol.* 2017,
586 4, 221-227, DOI: 10.1021/acs.estlett.7b00143
- 587 Huang, X.; Song, Y.; Li, J.; Huo, Q.; Cai, X.; Zhu, T.; Hu, M.; Zhang, H. A high-resolution ammonia emission inventory
588 in China. *Global Biogeochem. Cy.* 2012, 26, 1030-1044, DOI: 10.1029/2011GB004161
- 589 Kang, Y.; Liu, M.; Song, Y.; Huang, X.; Yao, H.; Cai, X.; Zhang, H.; Kang, L.; Liu, X.; Yan, X.; He, H.; Zhang, Q.; Shao,
590 M.; Zhu, T. High-resolution ammonia emissions inventories in China from 1980 to 2012. *Atmos. Chem. Phys.* 2016,
591 16, 2043-2058, DOI: 10.5194/acpd-15-26959-2015
- 592 Koo, B.; Wilson, G.; Morris, R.; Dunker, A.; Yarwood, G. Comparison of Source Apportionment and Sensitivity Analysis
593 in a Particulate Matter Air Quality Model. *Environ. Sci. Technol.* 2009, 43, 6669-6675
- 594 Kurokawa, J.; Ohara, T.; Morikawa, T.; Hanayama, S.; Maenhout, G.; Fukui, T.; Kawashima, K.; Akimoto, H. Emissions
595 of air pollutants and greenhouse gases over Asian regions during 2000-2008: Regional Emission inventory in ASia
596 (REAS) version 2. *Atmos. Chem. Phys.* 2013, 13, 11019-11058, DOI: 10.5194/acp-13-11019-2013
- 597 Kulmala, M.; Korhonen, P.; Napari, I.; Karlsson, A.; Berresheim, H.; O'Dowd, C. D. Aerosol formation during
598 PARFORCE: Ternary nucleation of H₂SO₄, NH₃, and H₂O. *J. Geophys. Res.* 2002, 107, DOI: 10.1029/2001JD000900.
- 599 Lai, S.; Zhao, Y.; Ding, A.; Zhang, Y.; Song, T.; Zheng, J.; Ho, K. F.; Lee, S.; Zhong, L. Characterization of PM_{2.5} and the
600 major chemical components during a 1-year campaign in rural Guangzhou. *Southern China, Atmos. Res.* 2016, 167,

601 208-215, DOI: 10.1016/j.atmosres.2015.08.007

602 Lei, Y.; Zhang, Q.; He, K.; Streets, D. Primary anthropogenic aerosol emission trends for China, 1990-2005. *Atmos. Chem.*

603 *Phys.* 2011, 11, 931-954, DOI: 10.5194/acp-11-931-2011

604 Liu, M.; Huang, X.; Song, Y.; Tang, J.; Cao, J.; Zhang, X.; Zhang, Q.; Wang, S.; Xu, T.; Kang, L.; Cai, X.; Zhang, H.;

605 Yang, F.; Wang, H.; Yu, J.; Lau, A.; He, L.; Huang, X.; Duan, L.; Ding, A.; Xue, L.; Gao, J.; Liu, B.; Zhu, T. Ammonia

606 emission control in China would mitigate haze pollution and nitrogen deposition, but worsen acid rain. *PNAS*, 2019,

607 116, 7760-7765, DOI: 10.1073/pnas.1814880116

608 Lu, Z.; Zhang, Q.; Streets, D. G. Sulfur dioxide and primary carbonaceous aerosol emissions in China and India, 1996-

609 2010. *Atmos. Chem. Phys.* 2011, 11, 9839-9864, DOI:

610 Mathur, R.; Yu, S.; Kang, D.; Schere, K. Assessment of the winter-time performance of developmental particulate matter

611 forecasts with the Eta-CMAQ modeling system. *J. Geophys. Res.* 2008, 113, DOI: 10.1029/2007JD008580,

612 McMurry, P. H.; Takano, H.; Anderson, G. R. Study of the ammonia (gas)-sulfuric acid (aerosol) reaction rate. *Environ.*

613 *Sci. Technol.* 1983, 17, 347-352, DOI: 10.1021/es00112a008

614 Paulot, F.; Jacob, D. J.; Pinder, R. W.; Bash, J. O.; Travis, K.; Henze, D. K. Ammonia emissions in the United States,

615 European Union, and China derived by high-resolution inversion of ammonium wet deposition data: Interpretation

616 with a new agricultural emissions inventory (MASAGE_NH3). *J. Geophys. Res.* 2014, 119, 4343-4364, DOI:

617 10.1002/2013JD021130

618 Pen, Y.; Tian, S.; Zhao, Y.; Zhang, L.; Zhu, X.; Gao, J.; Huang, W.; Zhou, Y.; Song, Y.; Zhang, Q.; Wang, Y. Identifying

619 ammonia hotspots in China using a national observation network. *Environ. Sci. Technol.* 2008, doi:

620 10.1021/acs.est.7b05235, DOI: 10.1021/acs.est.7b05235

621 Quan, J.; Tie, X.; Zhang, Q.; Liu, Q.; Li, X.; Gao, Y.; Zhao, D. Characteristics of heavy aerosol pollution during the 2012-

622 2013 winter in Beijing, China. *Atmos. Environ.* 2014, 88, 83-89, DOI: 10.1016/j.atmosenv.2014.01.058

623 Ren, H.; Zhang, L.; Hong, X. Politic recommendations on strengthening reduction of air pollutant emissions in China.

624 *Environ. Sustain. Dev.* 2014, 39, 4-13, (in Chinese)

625 Tao, M.; Chen, L.; Xiong, X.; Zhang, M.; Ma, P.; Tao, J.; Wang, Z. Formation process of the widespread extreme haze

626 pollution over northern China in January 2013: Implications for regional air quality and climate. *Atmos. Environ.*

627 2014, 98, 417-425, DOI: 10.1016/j.atmosenv.2014.09.026

628 Tanner, R. L.; Leaderer, B. P.; Spengler, J. D. Acidity of atmospheric aerosols. *Environ. Sci. Technol.* 1981, 15, 1150-1153,

629 DOI: 10.1021/es00092a003

630 van der Werf, G.; Randerson, J. Giglio, L.; Collatz, G.; Mu, M.; Kasibhatla, P.; Morton, D.; Defries, R.; Jin, Y.; van

631 Leeuwen, T. Global fire emissions and the contribution of deforestation, savanna, forest, agricultural, and peat fires

632 (1997-2009). *Atmos. Chem. Physics.* 2010, 10, 11707-11735, DOI: 10.5194/acp-10-11707-2010

633 Wang, G.; Zhang, R.; Gomez, M. E.; Yang, L.; Levy Zamora, M.; Hu, M.; Lin, Y.; Peng, J.; Guo, S.; Meng, J.; Li, J.;

634 Cheng, C.; Hu, T.; Ren, Y.; Wang, Y.; Gao, J.; Cao, J.; An, Z.; Zhou, W.; Li, G.; Wang, J.; Tian, P.; Marrero-Ortiz, W.;

635 Secret, J.; Du, Z.; Zheng, J.; Shang, D.; Zeng, L.; Shao, M.; Wang, W.; Huang, Y.; Wang, Y.; Zhu, Y.; Li, Y.; Hu, J.;

636 Pan, B.; Cai, L.; Cheng, Y.; Ji, Y.; Zhang, F.; Rosenfeld, D.; Liss, P. S.; Duce, R. A.; Kolb, C. E.; Molina, M. J.

637 Persistent sulfate formation from London Fog to Chinese haze. *Proc. Natl. Acad. Sci.* 2016, 113, 13630-13635, DOI:

638 10.1073/pnas.1616540113

639 Wang, H.; Qiao, L.; Lou, S.; Zhou, M.; Ding, A.; Huang, H.; Chen, J.; Wang, Q.; Tao, S.; Chen, C.; Li, L.; Huang, C.;

640 2016, Chemical composition of PM_{2.5} and meteorological impact among three years in urban Shanghai, China. *J.*

641 *Clean. Prod.* 2016, 112, 1302-1311, DOI: 10.1016/j.jclepro.2015.04.099

642 Wang, S.; Zhang, Q.; Martin, R.V.; Philip, S.; Liu, F.; Li, M.; Jiang, X.; He, K. Satellite measurements oversee China's

643 sulfur dioxide emission reductions from coal-fired power plants. *Environ. Res. Lett.* 2015, 10, doi: 10.1088/1748-

644 9326/10/11/114015, DOI:

645 Wang, S.; Xing, J.; Jang, C.; Zhu, Y.; Fu, J.; Hao, J. Impact Assessment of Ammonia Emissions on Inorganic Aerosols in
646 East China Using Response Surface Modeling Technique. *Environ. Sci. Technol.* 2011, 45, 9293-9300, DOI:
647 10.1021/es2022347

648 Wang, Z.; Chien, C.; Tonnesen, G. Development of a tagged species source apportionment algorithm to characterize three-
649 dimensional transport and transformation of precursors and secondary pollutants. *J. Geophys. Res.* 2009, 114, DOI:
650 10.1029/2008JD010846,

651 Whitten, G.; Heo, G.; Kimura, Y.; McDonald-Buller, E.; Allen, D.; Carter, W. P. L.; Yarwood, G. A new condensed toluene
652 mechanism for Carbon Bond: CB05-TU. *Atmos. Environ.* 2010, 44, 5346-5355, DOI:
653 10.1016/j.atmosenv.2009.12.029

654 Wu, S.; Hu, J.; Zhang, Y.; Aneja, V. P. Modeling atmospheric transport and fate of ammonia in North Carolina-Part II:
655 Effect of ammonia emissions on fine particulate matter formation. *Atmos. Environ.* 2008, 42, 3437-3451, DOI:
656 10.1016/j.atmosenv.2007.04.022

657 Xia, Y.; Zhao, Y.; and Nielsen, C. P. Benefits of China's efforts in gaseous pollutant control indicated by the bottom-up
658 emissions and satellite observations 2000-2014. *Atmos. Environ.* 2016, 136, 43-53, DOI:
659 10.1016/j.atmosenv.2016.04.013

660 Xu, P.; Liao, Y. J.; Lin, Y. H.; Zhao, C. X.; Yan, C. H.; Cao, M. N.; Wang, G. S.; Luan, S. J. High-resolution inventory of
661 ammonia emissions from agricultural fertilizer in China from 1978 to 2008. *Atmos. Chem. Phys.* 2016, 16, 1207-
662 1218, DOI: 10.5194/acpd-15-25299-2015

663 Yang, Y.; Wilkinson, J.; Russell, A. Fast, Direct Sensitivity Analysis of Multi-Dimensional Photochemical Models.
664 *Environ. Sci. Technol.* 1997, 31, 2859-2868, DOI: 10.1021/es970117w

665 Zhao, Z.; Bai, Z.; Winiwarter, W.; Kiesewetter, G.; Heyes, C.; Ma, L. Mitigating ammonia emission from agriculture
666 reduces PM_{2.5} pollution in the Hai River Basin in China. *Sci. Total Environ.* 2017, 609, 1152-1160, DOI:
667 10.1016/j.scitotenv.2017.07.240

668 Zhao, X. J.; Zhao, P. S.; Xu, J.; Meng, W.; Pu, W. W.; Dong, F.; He, D.; Shi, Q. F. Analysis of a winter regional haze event
669 and its formation mechanism in the North China Plain. *Atmos. Chem. Phys.* 2013, 13, 5685-5696, DOI: 10.5194/acp-
670 13-5685-2013

671 Zhang, J. K.; Sun, Y.; Liu, Z. R.; Ji, D. S.; Hu, B.; Liu, Q.; Wang, Y. S. Characterization of submicron aerosols during a
672 month of serious pollution in Beijing, 2013. *Atmos. Chem. Phys.* 2014, 14, 2887-2903, DOI: 10.5194/acp-14-2887-
673 2014.

674 Zhang, K.; Ma, Y.; Xin, J.; Liu, Z.; Ma, Y.; Gao, D.; Wu, J.; Zhang, W.; Wang, Y.; Shen, P. The aerosol optical properties
675 and PM_{2.5} components over the world's largest industrial zone in Tangshan, North China. *Atmos. Res.* 2018, 201, 226-
676 234, DOI: 10.1016/j.atmosres.2017.10.025

677 Zhang, L.; Chen, Y.; Zhao, Y.; Henze, D.; Zhu, L.; Song, Y.; Paulot, F.; Liu, X.; Pan, Y.; Lin, Y.; Huang, B. Agricultural
678 ammonia emissions in China: reconciling bottom-up and top-down estimates. *Atmos. Chem. Phys.* 2018, 18, 339-355,
679 DOI: 10.5194/acp-18-339-2018

680 Pan, Y.; Tian, S.; Zhao, Y.; Zhang, L.; Zhu, X.; Gao, J.; Huang, W.; Zhou, Y.; Song, Y.; Zhang, Q.; Wang, Y. Identifying
681 ammonia hotspots in China using a national observation network. *Environ. Sci. Technol.* 2018, doi:
682 10.1021/acs.est.7b05235, DOI: 10.1021/acs.est.7b05235

683 Zhang, X.; Wang, Y.; Niu, Y.; Zhang, X.; Gong, S.; Zhang, Y.; Sun, J. Atmospheric aerosol compositions in China:
684 spatial/temporal variability, chemical signature, regional haze distribution and comparisons with global aerosols.
685 *Atmos. Chem. Phys.* 2012, 12, 779-799, DOI: 10.5194/acp-12-779-2012

686 Zhou, F.; Ciais, P.; Hayashi, K.; Galloway, J.; Kim, D.; Yang, L.; Li, S.; Liu, B.; Shang, Z.; Gao, S. Re-estimating NH₃
687 emissions from Chinese cropland by a new nonlinear model. *Environ. Sci. Technol.* 2016, 50, 564-572, DOI:
688 10.1021/acs.est.5b03156

689 Zhou, Y.; Cheng, S.; Lang, J.; Chen, D.; Zhao, B.; Liu, C.; Xu, R.; Li, T. A comprehensive ammonia emission inventory
690 with high-resolution and its evaluation in the Beijing–Tianjin–Hebei (BTH) region, China. *Atmos. Environ.* 2015,
691 106, 305-317, DOI: 10.1016/j.atmosenv.2015.01.069

692 Xu, P.; Koloutsou-Vakakis, S.; Rood, M.; Luan, S. Projections of NH₃ emissions from manure generated by livestock
693 production in China to 2030 under six mitigation scenarios. *Sci. Total Environ.* 2017, 31, 78-86, DOI:
694 10.1016/j.scitotenv.2017.06.258

695 Zheng, B.; Tong, D.; Li, M.; Liu, F.; Hong, C.; Geng, G.; Li, H.; Li, X.; Peng, L.; Qi, J.; Yan, L.; Zhang, Y.; Zhao, H.;
696 Zheng, Y.; He, K.; Zhang, Q. Trends in China's anthropogenic emissions since 2010 as the consequence of clean air
697 actions. *Atmos. Chem. Phys.* 2018, 18, 14095-14111, DOI: 10.5194/acp-18-14095-2018

698 Kurokawa, J.; Ohara, T.; Morikawa, T.; Hanayama, S.; Janssens-Maenhout, G.; Fukui, T.; Kawashima, K.; Akimoto, H.
699 Emissions of air pollutants and greenhouse gases over Asian regions during 2000-2008: Regional Emission inventory
700 in ASia (REAS) version 2. *Atmos. Chem. Phys.* 2013, 13, 11019-11058, DOI: 10.5194/acp-13-11019-2013

701 Fu, X.; Wang, S.; Ran, L.; Pleim, J.; Cooter, E.; Bash, J.; Benson, V.; Hao, J. Estimating NH₃ emissions from agricultural
702 fertilizer application in China using the bi-directional CMAQ model coupled to an agro-ecosystem model. *Atmos.*
703 *Chem. Phys.* 2015, 15, 6637-6649, DOI: 10.5194/acp-15-6637-2015

704

705

706

707

708

709

710

711

712

713

714

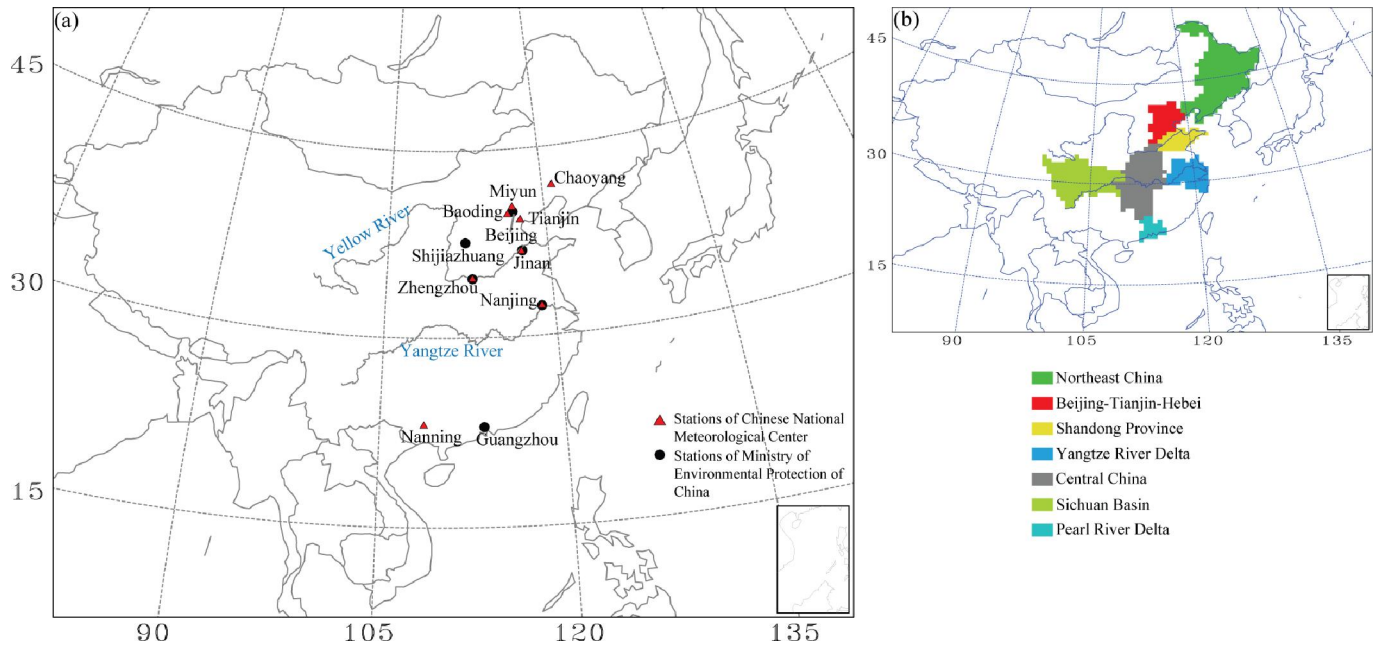
715

716

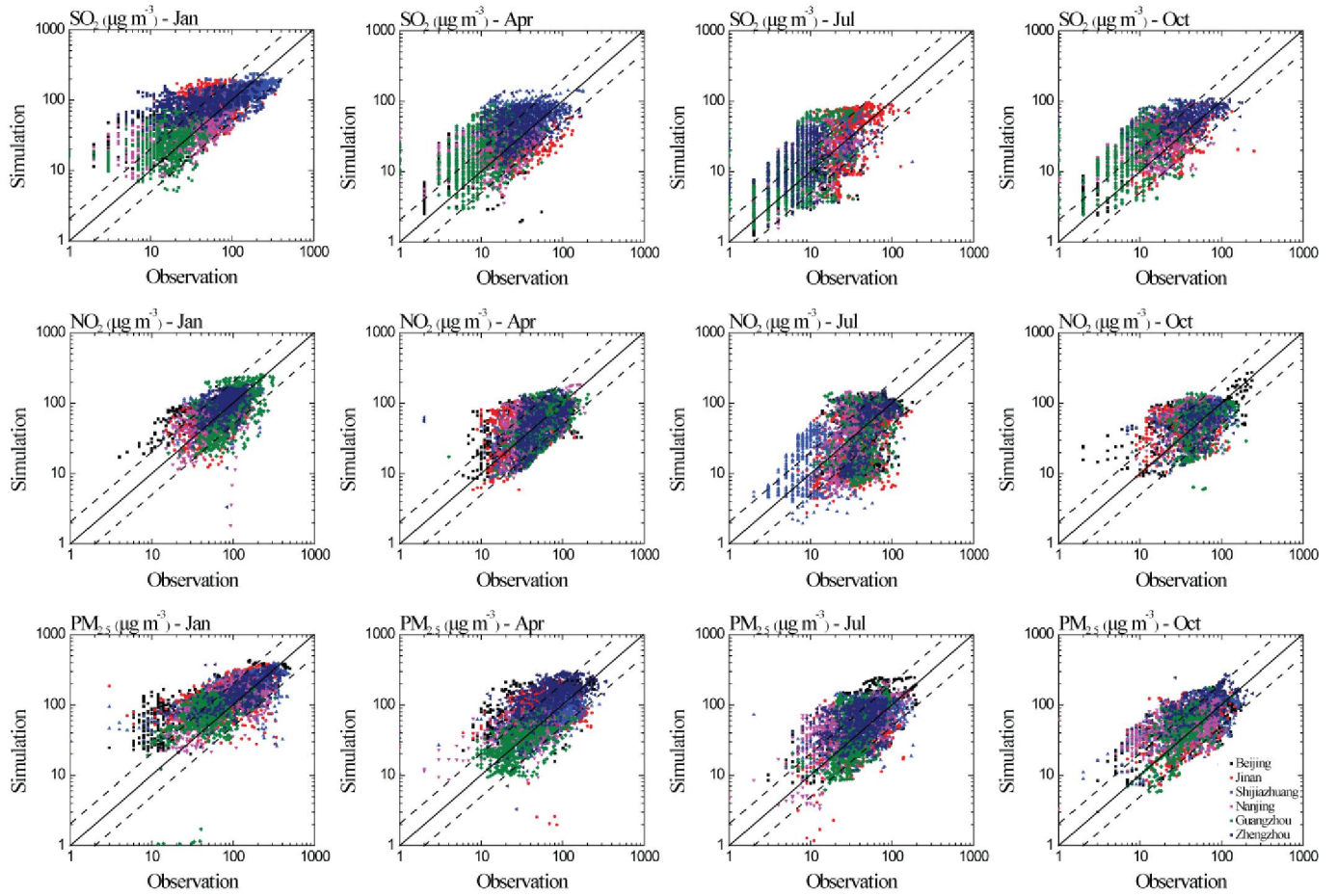
717

718

719

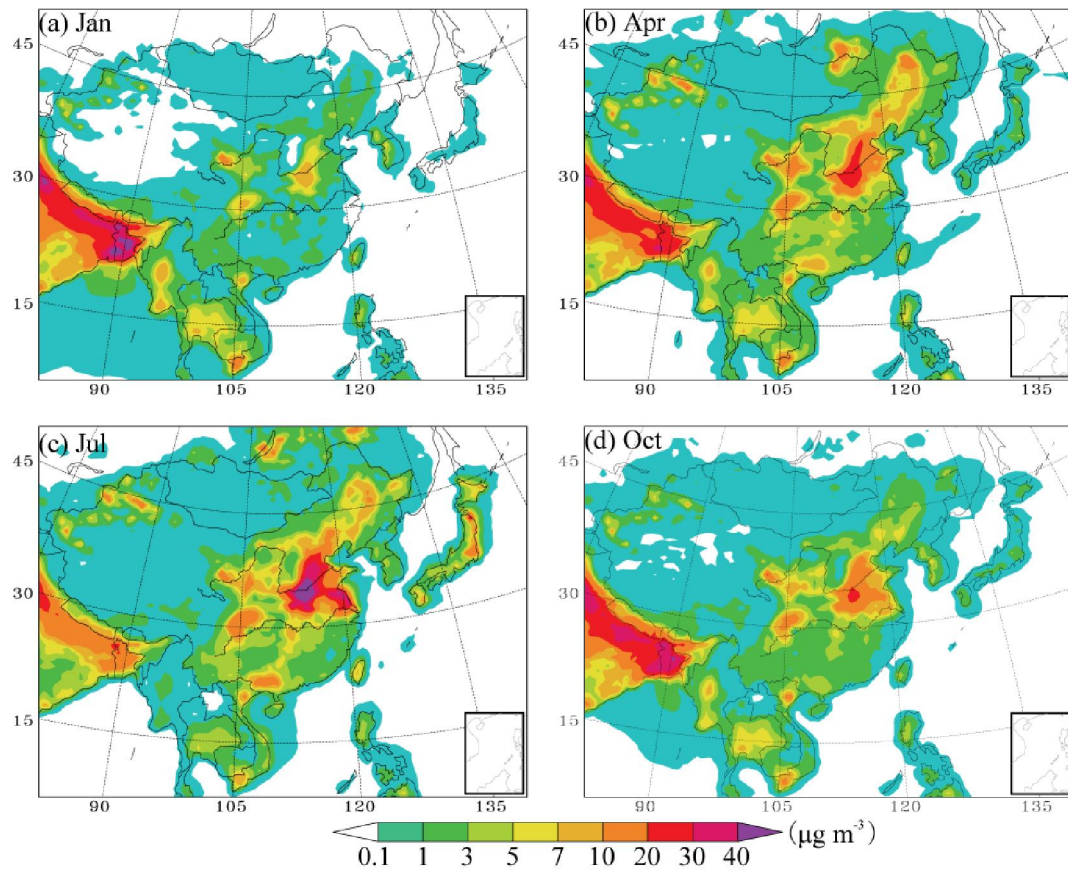


720
 721 **Figure 1. Model domain used in this study and the geographic locations of Beijing-Tianjin-Hebei (BTH), Northeast**
 722 **China (NEC), Yangtze River Delta (YRD), Pearl River Delta (PRD), Sichuan Basin (SCB), Central China (CNC) and**
 723 **Shandong Province (SDP). The location of observation data was also shown in the model domain.**
 724
 725
 726
 727
 728
 729
 730
 731
 732
 733
 734
 735
 736
 737
 738
 739
 740
 741
 742
 743
 744
 745
 746
 747
 748

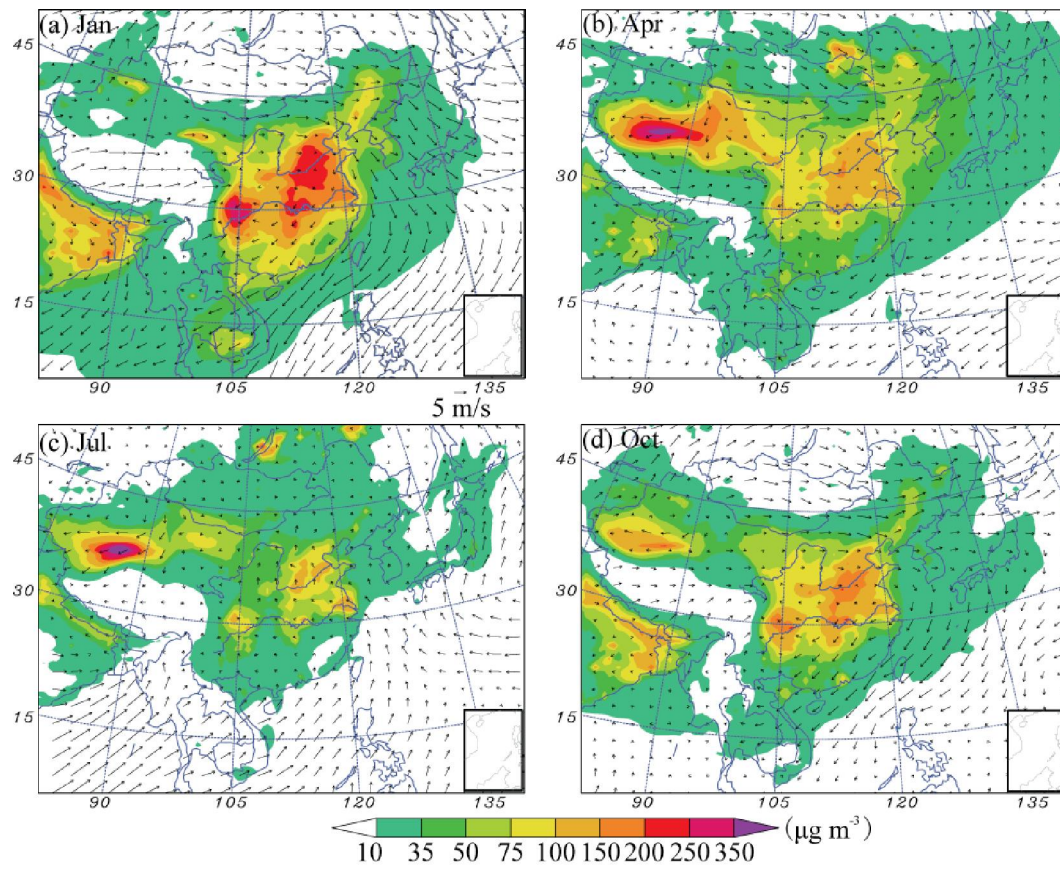


749
 750 **Figure 2.** The scatter plots between the modeled and the observed hourly SO₂, NO₂, and PM_{2.5} in January, April, July and
 751 **October 2015.** The solid lines are 1:1 and the dashed lines are 2:1 or 1:2.

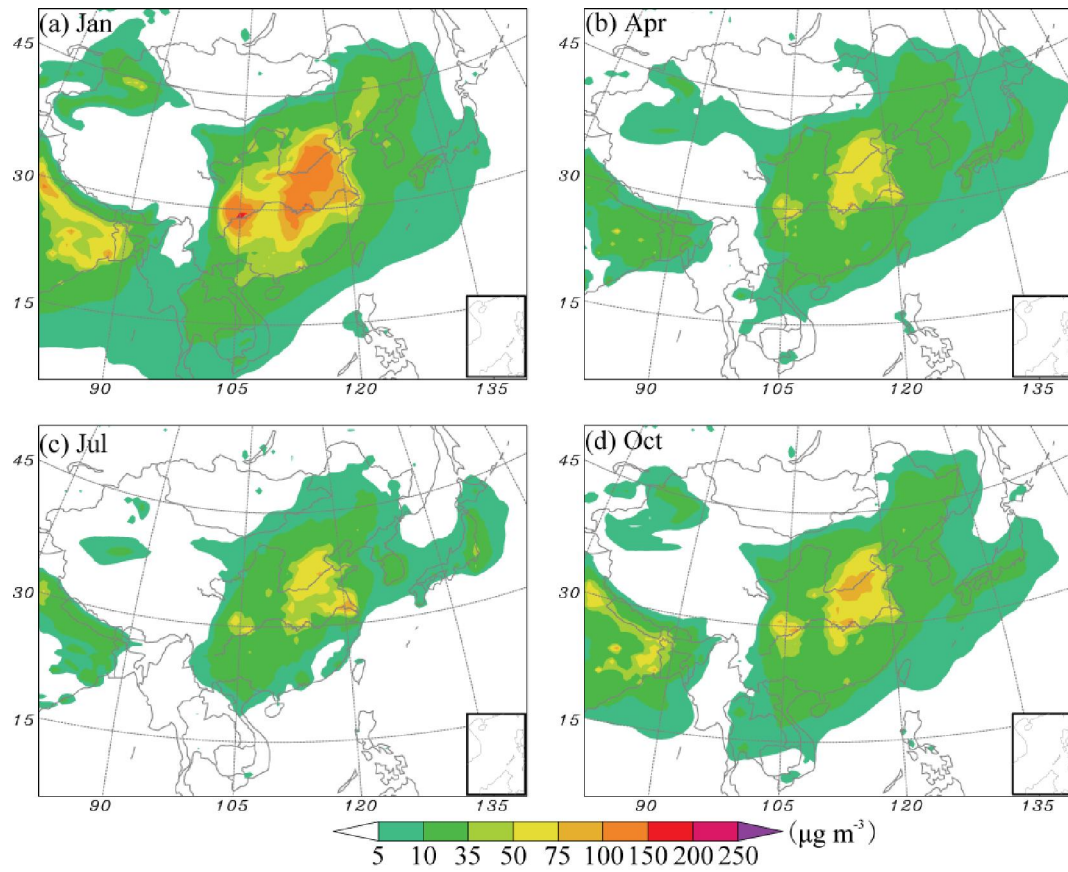
749
 750
 751
 752
 753
 754
 755
 756
 757
 758
 759
 760
 761
 762
 763
 764
 765
 766
 767
 768
 769
 770



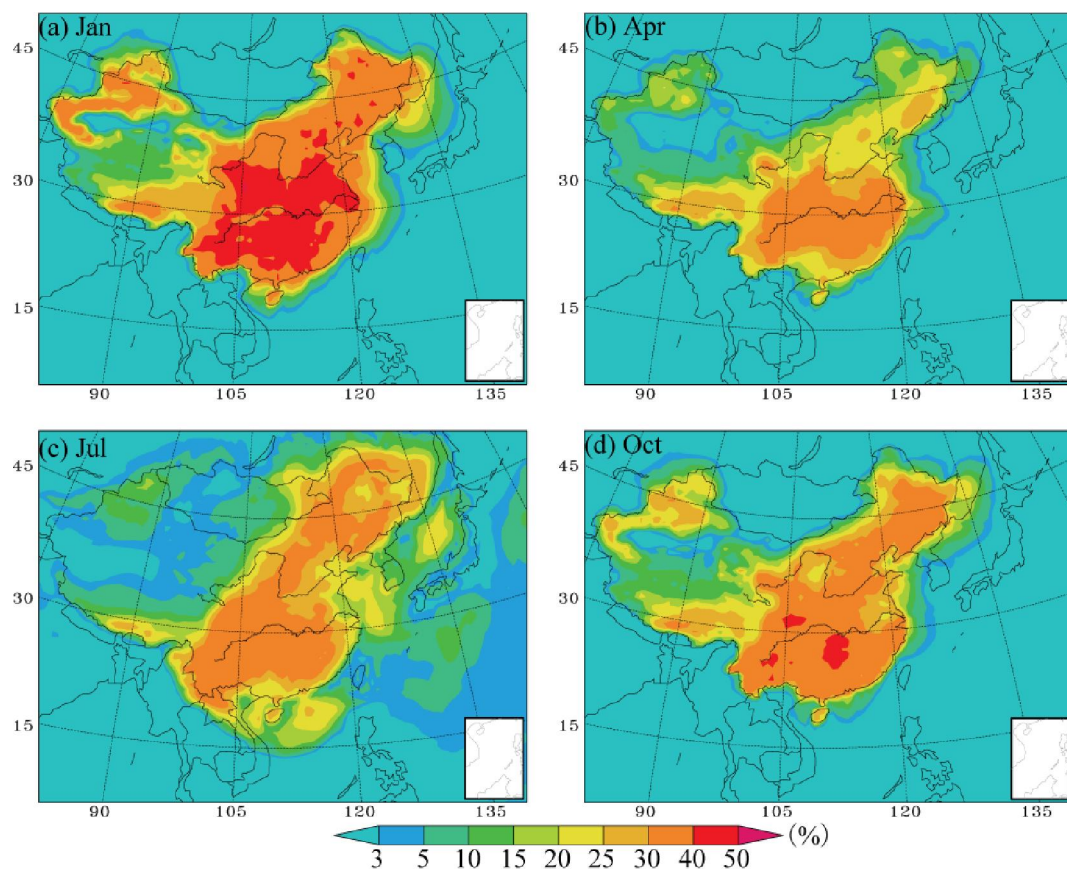
771
 772 Figure 3. The horizontal distributions of the modeled monthly NH_3 mass concentration in January, April, July, and
 773 October in 2015.
 774
 775
 776
 777
 778
 779
 780
 781
 782
 783
 784
 785
 786
 787
 788
 789
 790
 791
 792
 793



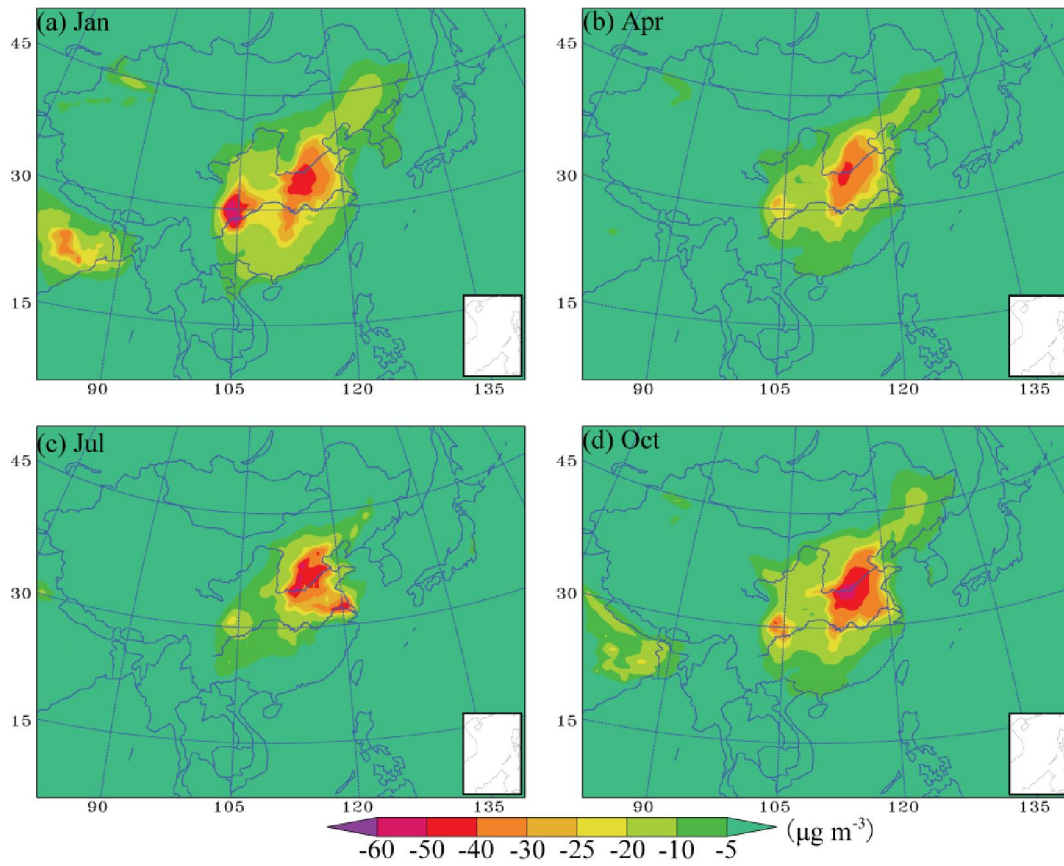
794
 795 Figure 4. The horizontal distributions of the modeled monthly PM_{2.5} mass concentration in January, April, July, and
 796 October in 2015. Also shown are the surface wind field.
 797
 798
 799
 800
 801
 802
 803
 804
 805
 806
 807
 808
 809
 810
 811
 812
 813
 814
 815
 816
 817



818
 819 Figure 5. The horizontal distributions of the modeled monthly SNA mass concentration in January, April, July, and
 820 October in 2015.
 821
 822
 823
 824
 825
 826
 827
 828
 829
 830
 831
 832
 833
 834
 835
 836
 837
 838
 839
 840
 841



842
 843 **Figure 6. The horizontal distributions of the contribution percentage of NH_3 emissions to SNA mass concentration (%) in**
 844 **January, April, July and October.**
 845
 846
 847
 848
 849
 850
 851
 852
 853
 854
 855
 856
 857
 858
 859
 860
 861
 862
 863
 864
 865



866
 867 **Figure 7. The horizontal distributions of SNA mass concentration ($\mu\text{g m}^{-3}$) variation associated with agriculture NH_3**
 868 **removal in January, April, July and October.**
 869

870
 871
 872
 873
 874
 875
 876
 877
 878
 879
 880
 881
 882
 883
 884
 885
 886
 887
 888
 889

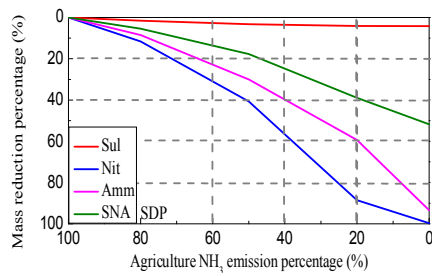
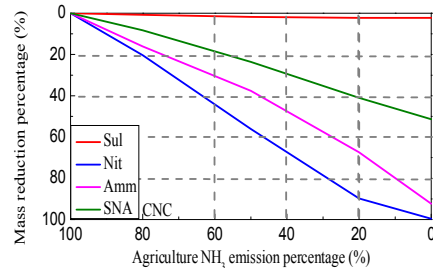
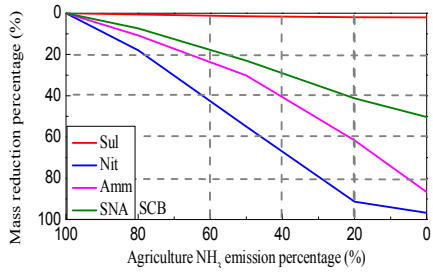
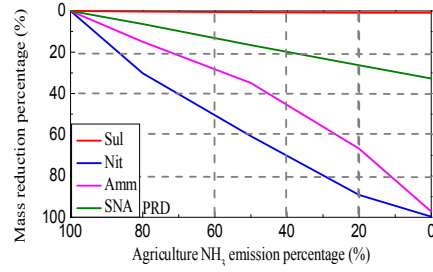
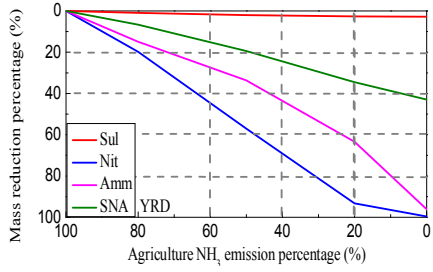
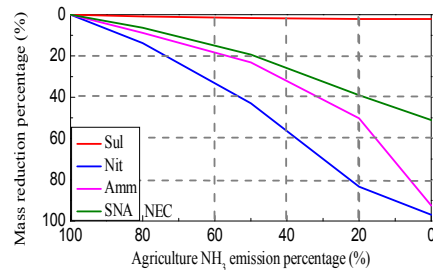
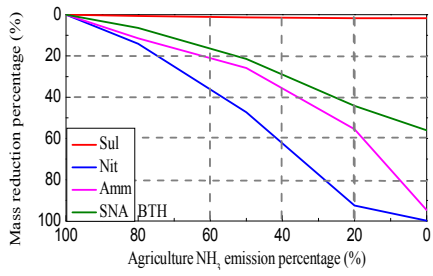


Figure 8. The variation (%) of sulfate, nitrate, ammonium, and SNA mass burden associated with the NH₃ emission reduction (%).

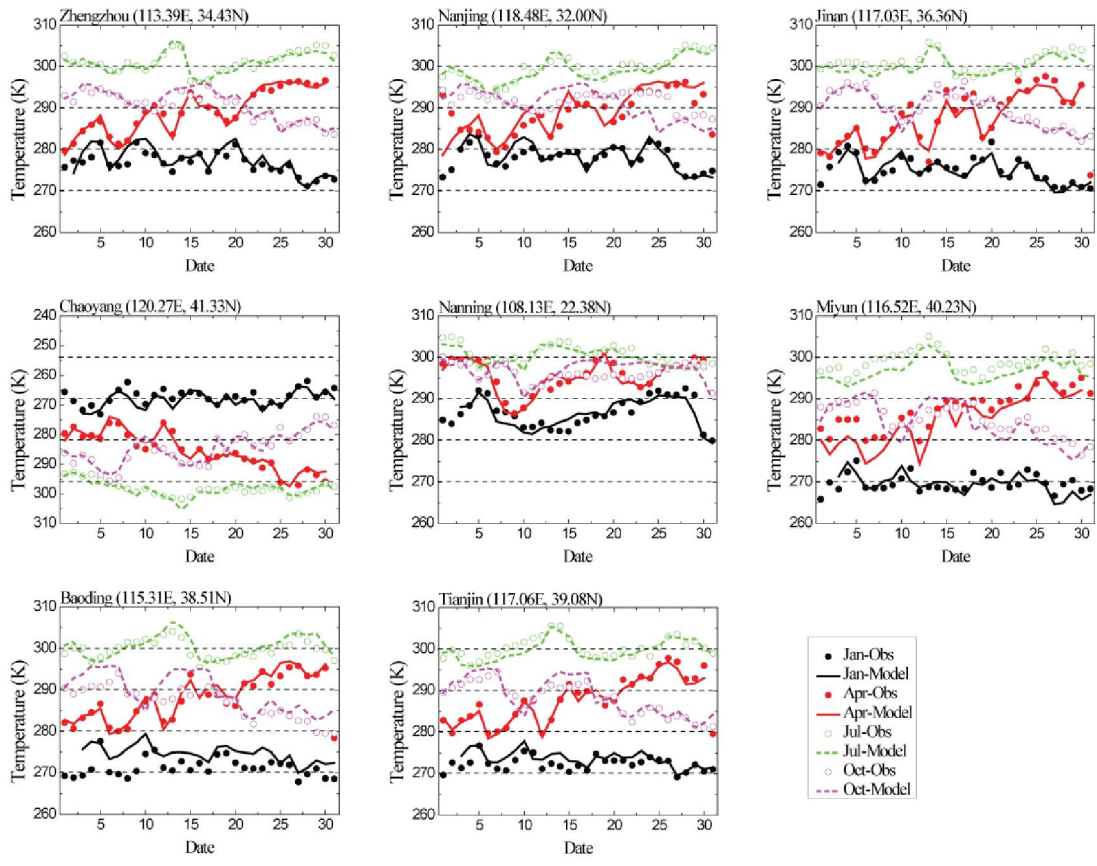


Figure A1. Observed and modeled daily average temperatures (K) in January, April, July and October 2015.

908
 909
 910
 911
 912
 913
 914
 915
 916
 917
 918
 919
 920
 921
 922
 923
 924
 925
 926
 927
 928
 929
 930

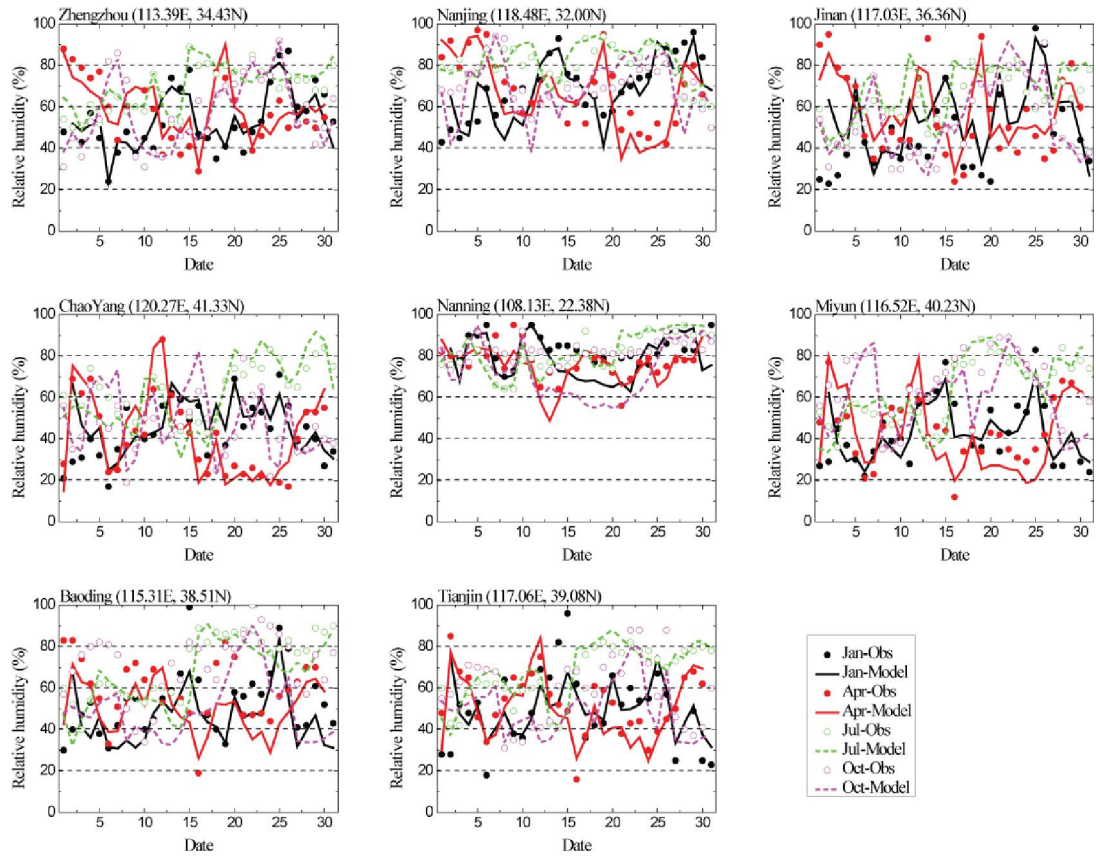


Figure A2. Same as Figure A1 but for relative humidity (%)

931
 932
 933
 934
 935
 936
 937
 938
 939
 940
 941
 942
 943
 944
 945
 946
 947
 948
 949
 950
 951
 952
 953
 954

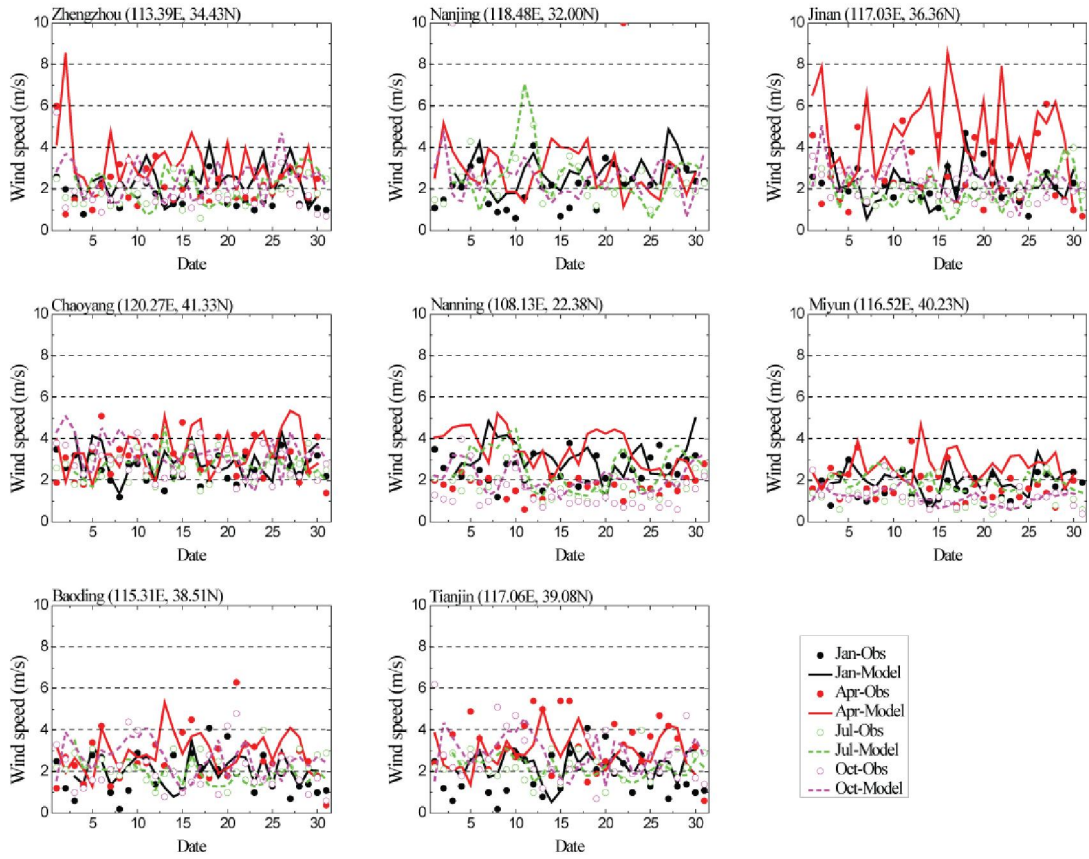


Figure A3. Same as Figure A1 but for wind speed (m s^{-1})

955
 956
 957
 958
 959
 960
 961
 962
 963
 964
 965
 966
 967
 968
 969
 970
 971
 972
 973
 974
 975
 976
 977
 978

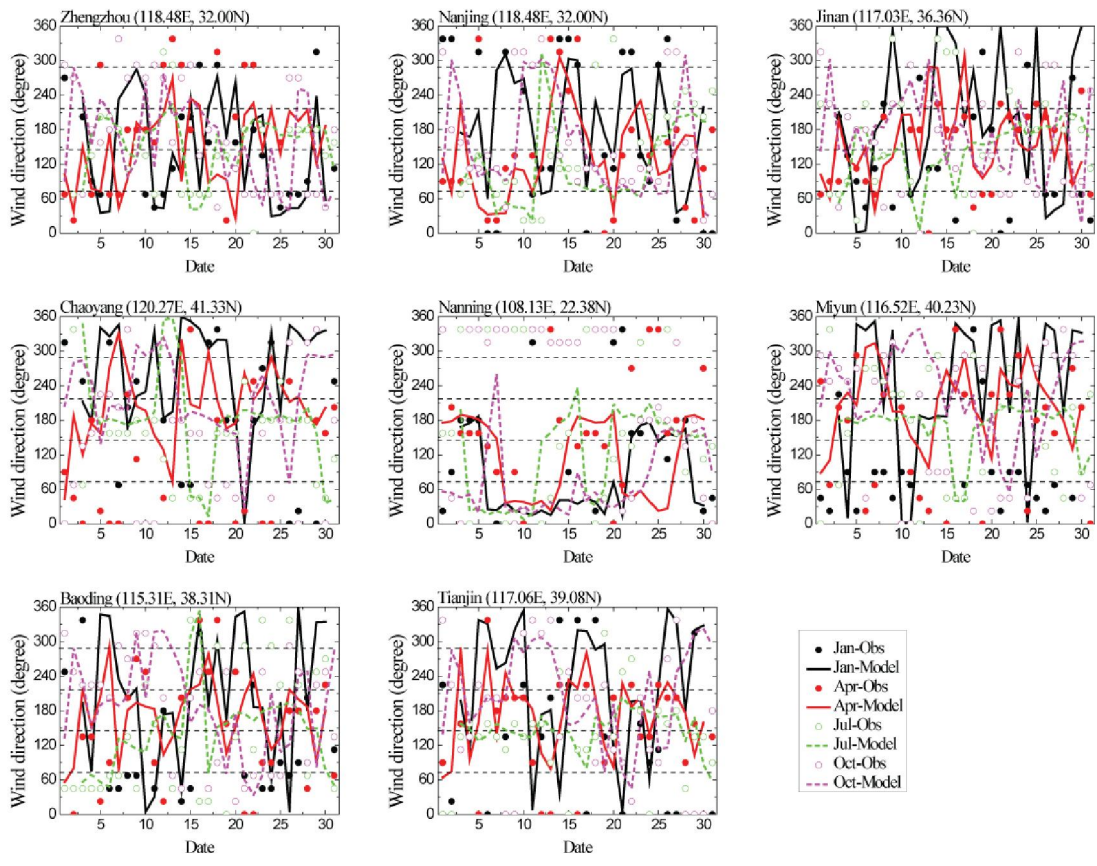


Figure A4. Same as Figure A1 but for daily maximum wind direction (degree)

979
 980
 981
 982
 983
 984
 985
 986
 987
 988
 989
 990
 991
 992
 993
 994
 995
 996
 997
 998
 999
 1000
 1001
 1002

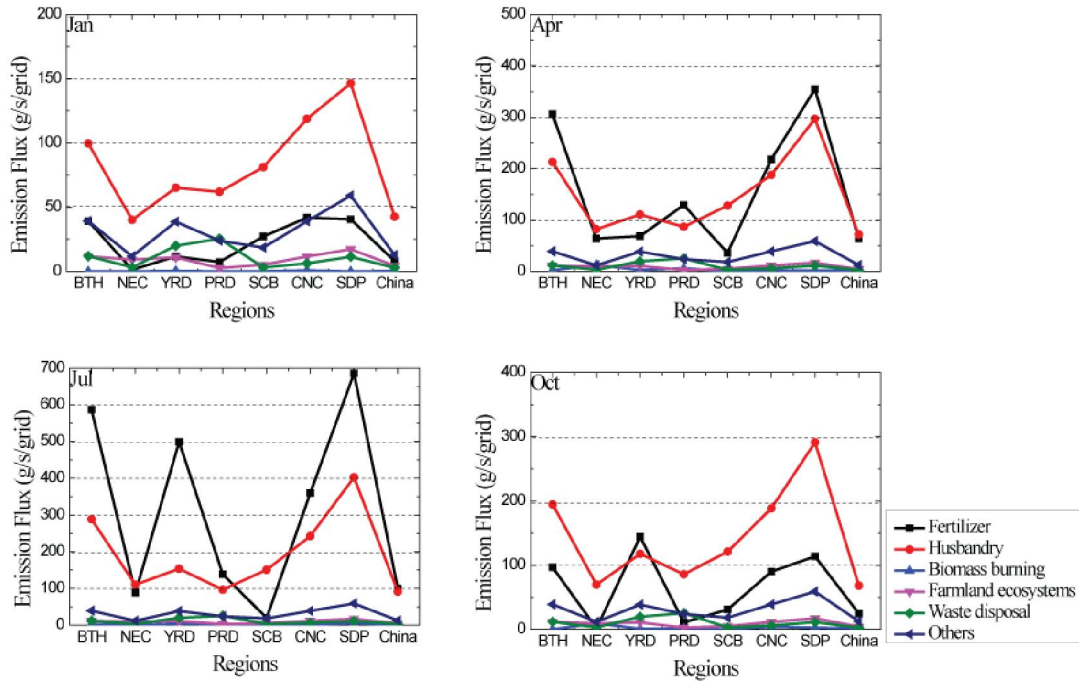


Figure A5. The regional average NH₃ emission flux (g/s/grid) of different agriculture sectors over each region in January, April, July and October.

1003
 1004
 1005
 1006
 1007
 1008
 1009
 1010
 1011
 1012
 1013
 1014
 1015
 1016
 1017
 1018
 1019
 1020
 1021
 1022
 1023
 1024
 1025
 1026
 1027
 1028
 1029
 1030

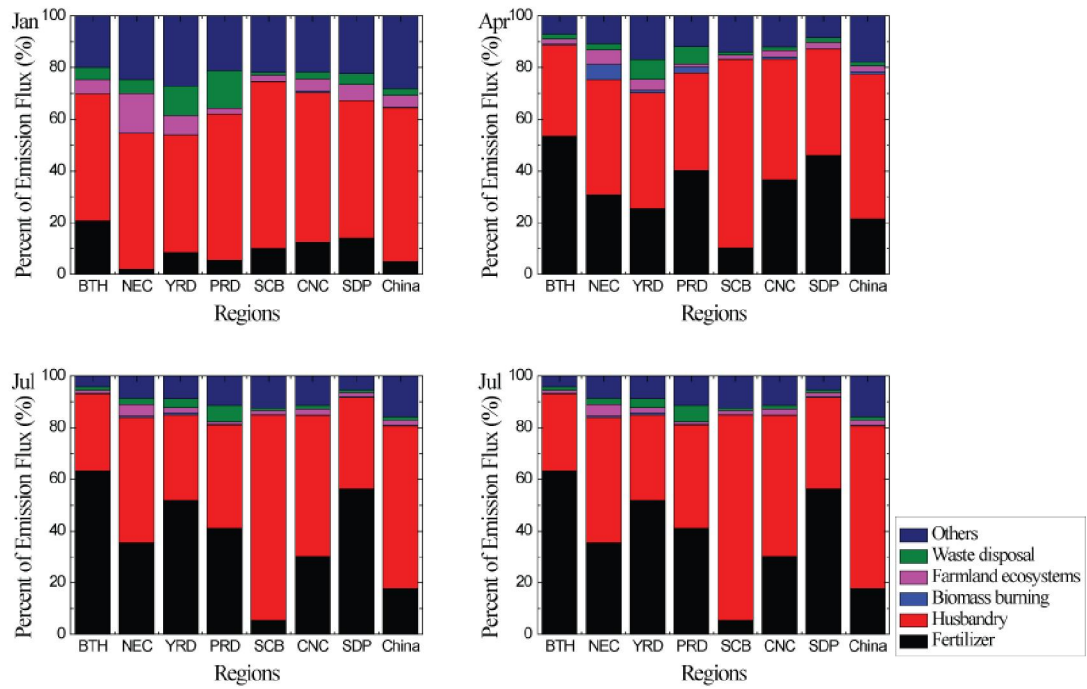


Figure A6. The percent (%) of different NH₃ emission sectors over each region in January, April, July and October.

1031
 1032
 1033
 1034
 1035
 1036
 1037
 1038
 1039
 1040
 1041
 1042
 1043
 1044
 1045
 1046
 1047
 1048
 1049
 1050
 1051
 1052
 1053
 1054
 1055
 1056
 1057
 1058

1059

Table 1. Statistical summary of the comparisons of the monthly average PM_{2.5} between simulation and observation

	N^a	O^b	M^c	σ_o^d	σ_m^e	R^f
Jan	4464	106.5	126.9	84.5	76.2	0.74
Apr	4320	64.6	76.8	44.7	56.8	0.66
Jul	4464	49.2	42.1	32.3	41.4	0.58
Oct	4464	58.2	68.1	35.5	46.9	0.61

1060

^a Number of samples

1061

^b Total mean of observation

1062

^c Total mean of simulation

1063

^d Standard deviation of observation

1064

^e Standard deviation of simulation

1065

^f Correlation coefficient between daily observation and simulation

1066

1067

1068

1069

1070

1071

1072

1073

1074

1075

1076

1077

1078

1079

1080

1081

1082

1083

1084

1085

1086

1087

1088

1089

1090

1091

1092

1093

1094

1095

1096

1097

1098

Table 2. Statistical summary of the comparisons of the monthly average NO₂ between simulation and observation

	<i>N</i>	<i>O</i>	<i>M</i>	σ_o	σ_m	<i>R</i>
Jan	4464	79.7	87.1	39.8	39.0	0.60
Apr	4320	53.7	55.5	29.9	32.5	0.59
Jul	4464	43.6	40.1	25.8	30.0	0.51
Oct	4464	53.6	61.3	32.0	31.7	0.54

1099
1100
1101
1102
1103
1104
1105
1106
1107
1108
1109
1110
1111
1112
1113
1114
1115
1116
1117
1118
1119
1120
1121
1122
1123
1124
1125
1126
1127
1128
1129
1130
1131
1132
1133
1134
1135
1136

1137

Table 3. Statistical summary of the comparisons of the monthly average SO₂ between simulation and observation

	<i>N</i>	<i>O</i>	<i>M</i>	σ_o	σ_m	<i>R</i>
Jan	4464	61.0	71.5	61.3	47.5	0.63
Apr	4320	24.8	35.7	26.5	24.6	0.52
Jul	4464	13.9	22.4	15.1	19.1	0.46
Oct	4464	21.2	36.8	20.2	21.8	0.50

1138
1139
1140
1141
1142
1143
1144
1145
1146
1147
1148
1149
1150
1151
1152
1153
1154
1155
1156
1157
1158
1159
1160
1161
1162
1163
1164
1165
1166
1167
1168
1169
1170
1171
1172
1173
1174
1175

Table 4. The regional percent (%) of Tagr NH₃ contribution to sulfate, nitrate, ammonium, and SNA mass concentration.

		Sulfate	Nitrate	Ammonium	SNA	PM _{2.5}
BTH	Jan	0.9	4.5	98.0	39.7	19.3
	Jul	1.0	9.3	75.9	28.1	20.6
	Annual	1.1	8.0	83.3	23.1	15.5
NEC	Jan	0.6	3.2	94.0	34.4	18.6
	Jul	0.8	6.7	83.5	27.9	16.1
	Annual	1.0	5.6	83.7	22.5	14.3
YRD	Jan	0.9	5.8	99.2	40.9	22.5
	Jul	0.5	8.1	68.7	24.0	15.4
	Annual	1.0	7.4	85.7	23.6	15.3
PRD	Jan	0.8	5.0	98.1	40.2	20.4
	Jul	1.4	4.7	85.3	27.7	15.9
	Annual	0.9	5.8	90.6	24.5	14.2
SCB	Jan	0.6	3.7	97.0	37.4	17.9
	Jul	0.7	5.6	95.9	31.5	19.5
	Annual	0.7	5.1	93.9	21.6	13.0
CNC	Jan	0.9	4.9	99.2	42.6	20.6
	Jul	0.9	6.7	88.9	33.7	22.0
	Annual	0.9	6.0	92.8	26.1	17.5
SDP	Jan	0.7	4.9	98.3	39.2	21.0
	Jul	0.7	8.3	67.0	23.5	16.6
	Annual	0.9	7.1	80.5	21.6	15.1
China	Jan	2.4	9.3	92.3	34.4	21.4
	Jul	2.2	10.4	90.9	25.1	16.4
	Annual	2.2	10.1	87.6	29.0	16.0

1177

1178

1179

1180

1181

1182

1183

1184

1185

1186

1187

1188

1189

1190

1191

1192

1193

1194

1195
1196

Table 5. The variation percent (%) of sulfate, nitrate, ammonium, and SNA mass concentration associated with agriculture NH₃ removal.

		Sulfate	Nitrate	Ammonium	SNA	PM _{2.5}
BTH	Jan	0.5	99.8	96.2	51.9	37.8
	Jul	1.0	99.6	95.0	47.0	39.2
	Annual	0.7	99.8	94.7	49.4	38.5
NEC	Jan	0.7	99.2	96.4	60.9	39.2
	Jul	0.8	94.5	91.5	37.0	27.8
	Annual	0.7	96.9	92.5	48.9	34.5
YRD	Jan	2.7	99.4	96.0	52.6	32.2
	Jul	7.2	99.0	96.8	44.9	37.6
	Annual	5.0	99.2	96.1	48.8	36.9
PRD	Jan	3.6	99.8	97.2	50.3	31.5
	Jul	0.4	92.7	97.4	30.3	24.1
	Annual	2.0	96.2	97.2	40.3	27.8
SCB	Jan	4.9	94.1	80.3	57.6	41.7
	Jul	0.2	99.3	92.5	42.0	28.3
	Annual	2.6	96.7	85.9	49.8	35.0
CNC	Jan	3.1	99.1	92.2	56.7	41.5
	Jul	0.7	99.3	96.0	45.1	37.2
	Annual	1.9	99.2	92.3	50.9	39.4
SDP	Jan	1.7	99.8	95.8	47.7	38.0
	Jul	3.6	99.2	93.6	45.6	37.3
	Annual	2.7	99.5	93.4	46.6	37.6
China	Jan	2.6	93.9	86.3	54.8	39.5
	Jul	0.6	97.7	87.8	36.7	27.5
	Annual	1.6	95.8	86.9	45.7	32.9

1197
1198
1199
1200
1201